TÜBİTAK

Turkish Journal of Earth Sciences

http://journals.tubitak.gov.tr/earth/

Research Article

Turkish J Earth Sci
(2018) 27: 205-231

doi:10.3906/yer-1707-5

Cathodoluminescence, fluid inclusions, and trace element data for the syntaxial quartz cementation in the sandstones of the Ora Formation, northern Iraq

Muhamed F. OMER[1,2,*], Henrik FRIIS[3]

[1]Department of Geology, College of Science, Salahaddin University, Erbil, Iraq
[2]Faculty of Geology, Warsaw University, Warsaw, Poland
[3]Department of Geoscience, Aarhus University, Aarhus, Denmark

Received: 09.07.2017 • **Accepted/Published Online:** 25.12.2017 • **Final Version:** 17.05.2018

Abstract: Quartz cements of the quartz arenitic sandstones from the Chalky Nasara and Ora sections of the (Devonian-Carboniferous) Ora Formation in northern Iraq have been studied. A combination of hot cathodoluminescence, LA-ICP-MS, and fluid inclusion microthermometry revealed three syntaxial quartz cement generations (Q1, Q2, and Q3). The early Q1 cementation has gray to slightly brown luminescences, postdated compaction, and reduced intergranular porosity associated with illite formed during eogenesis. Q2 is characterized by dark brown luminescence overgrowths and is more voluminous in the thinly bedded sandstones than in the thickly bedded sandstones filling most of the remaining pore space during mesogenesis. Q3 was formed during the early telogenesis stage fully cementing the sandstones and the fractures were filled by hydrothermal chlorite and sulfides. Significant amounts of trace elements Al, Li, Ge, and Fe have been detected in quartz overgrowths. Al varies consistently between each cement with averages of 7125, 4044, and 2036 ppm for the Q1, Q2, and Q3 generations, respectively. A strong linear correlation between Al and Li in the three quartz cements with an average Li/Al of ~0.02 in Q1 and Q2 indicates sufficient availability of both Al and Li where Li is most likely to be found in high-saline pore waters. Illite is the most probable origin of Li since high salinities favor the mobilization of Li during diagenesis. Germanium concentrations in quartz cements are slightly less than that in the detrital quartz of the Ora Formation, indicating that the pressure dissolutions of quartz and feldspar are the dominant sources of cementation in the Ora Formation. Homogenization temperatures of fluid inclusions indicate precipitation of the Q1, Q2, and Q3 cement generations at temperature ranges of 155–160 °C, 160–166 °C, and 168–178 °C, respectively, with salinities ranging between 5.0 and 6.4 wt.% NaCl equiv., as an indication of hydrothermal burial conditions for Q3 cement, which was affected by the major Zagros Thrust Zone faulting.

Key words: Quartz cement generations, cathodoluminescence, trace elements, fluid inclusions, Ora Formation, northern Iraq

1. Introduction

Sandstones have been the target of a large number of studies because of their capability to become reservoirs for water and hydrocarbon (Marchand et al., 2002; Molenaar et al., 2008; Taylor et al., 2010). The evaluation of reservoir properties in deeply buried sandstones requires understanding the process and distribution of authigenically formed quartz, which has an important impact on the reduction of porosity and permeability of sandstones (Worden and Morad, 2000; Molenaar et al., 2007, 2008; Tamer-Agha, 2009). Important aspects are the estimation of formation temperatures of different phases of quartz cementation and their possible silica sources. Techniques for estimating the formation temperature of diagenetic quartz include oxygen isotope measurements by means of ion microprobe (Rezaee and Tingate, 1997; Hiatt et al., 2007; Kelly et al., 2007) and fluid inclusion studies (Roedder, 1984; Demars, et al., 1996; Kraishan et al., 2000). The rate of quartz cementation as a function of time, temperature, and the nature of the quartz surface can also be deduced from such studies (Walderhaug, 1994). Successive phases of quartz cementation and their possible silica sources may partly be revealed by trace element analyses of the quartz cement.

The most significant trace elements incorporated in authigenic and hydrothermal quartz grown at low temperatures are Al, Li, Na, and Ge (<300 °C; Bambauer, 1961; Lehmann et al., 2011; Götte et al., 2011, 2013). The Al content is believed to be related to the diagenesis of feldspars (Kraishan et al., 2000; Weber and Ricken, 2005). According to Lehmann et al. (2011), Ge is considered a proxy element for the silica source while the Al content is linked to the evolution of the pore water. Ge is considered to be a proxy element for the silica source and the Al

* Correspondence: muhfakhri2005@gmail.com

content is linked to the evolution of the pore water (Lehmann et al., 2011). Enrichment in Li may indicate transformation of clay minerals since they are the most important source of Li (Williams and Hervig, 2005). The cathodoluminescence (CL) of quartz strongly depends on the trace element distribution (Demars et al., 1996) and therefore may contribute to the understanding of various silica sources.

The Ora Formation (Upper Devonian-Carboniferous) has been subjected to a complicated geological evolution in terms of successive phases of burial, oogenesis, and uplift. The purpose of this study is to clarify the successive lithification of the Ora Formation during this evolution with emphasis on the development of quartz cement and identification of the related silica sources.

2. Geological setting and Late Paleozoic evolution

The siliciclastic Paleozoic successions of the Ora Formation were first recognized in the Northern Thrust Zone of northern Iraq, close to the Iraq–Turkey border, by Wetzel and Morten in 1952 (in Bellen et al., 1959) (Figure 1). The geological development of Iraq is controlled by its position within the main tectonic units of the Middle Eastern region, i.e. between the Arabian part of the African Platform (Nubio-Arabian) and the Asian branches of the Alpine Tectonic Belt.

Northern and northeastern Iraq is a part of the extensive Alpine-Himalyan Orogenic Belt in the Near East, represented by the Taurus-Zagros Mountain Belt, which was developed as a result of collision between the Afro-Arabian and Eurasian plates (Sharland et al., 2001). The Zagros Mountain Belt as part of the Alpine-Himalayan mountain chain is a well-defined asymmetric mountain belt (Alavi, 1994). The northwestern boundary of the Zagros Mountain Belt is chosen to be the East Anatolian Fault (EAF in Figure 2) in southeastern Turkey. This fault separates the Zagros from the Eastern Taurides of Turkey and offsets the two mountain belts left-laterally for ~300 km. The Zagros Mountain Belt consists of three tectonic zones, the Urumieh-Dokhtar Magmatic Assemblage; the Zagros Imbricate Zone, which includes both the Sanandaj-Sirjan Zone and the Zagros Thrust Zone of Stocklin (1968, 1974); and the Zagros Fold-Thrust Belt (Figure 2). The boundary between the Sanandaj-Sirjan Zone of Stocklin and his Zagros Thrust Zone (referred to as the "Main Zagros Thrust") has been regarded by many researchers as the suture between the Afro-Arabian and Iranian plates (Takin, 1972; Hessami et al., 2001; Talebian and Jackson, 2004). This zone includes folded and thrusted sediment from the former northeastern passive continental margin of the Afro-Arabian continent. Following this interpretation, the northeastern boundary of the Zagros Imbricate Zone, where the magmatic assemblage is juxtaposed against the Zagros Imbricate Zone, is considered to be suture zone between the Afro-Arabian and Iranian plates (ZS in Figure 2). According to

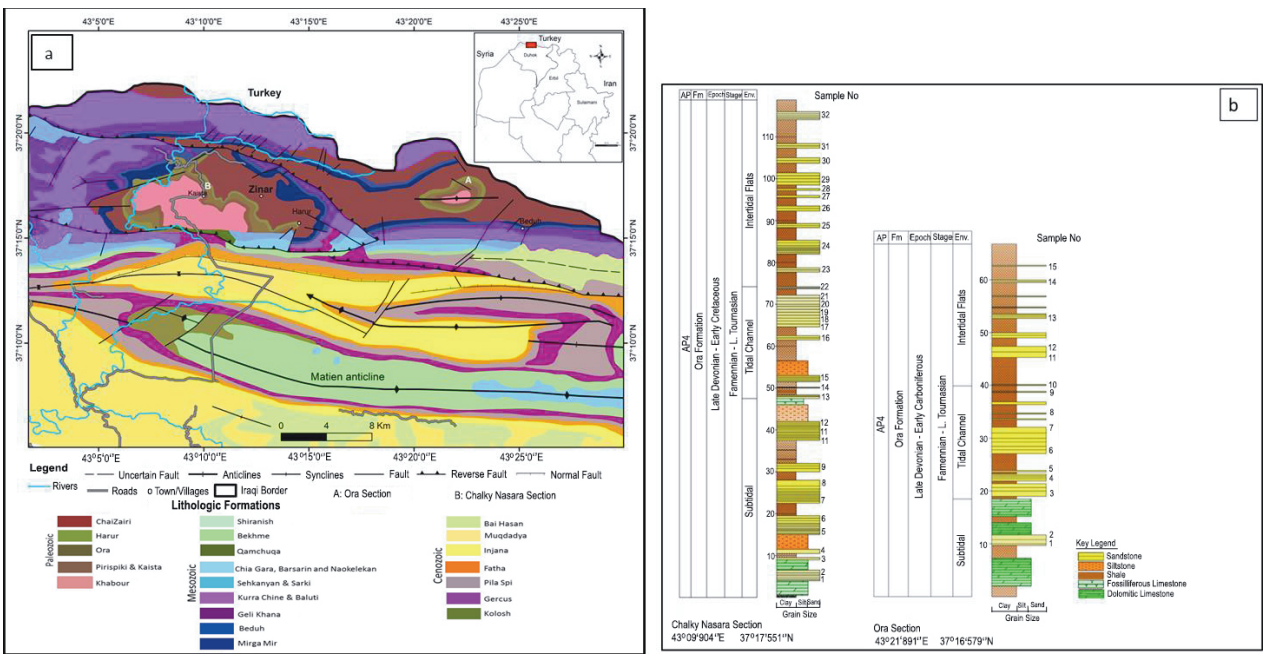

Figure 1. Geological map of northern Iraq showing the location of the studied clastic rocks in the Ora Formation and other Paleozoic rocks (modified after Sissakian, 2000) (a). Columnar sections of the Ora Formation in two outcrop sections, Chalky Nasara and Ora sections, with locations of selected samples (b).

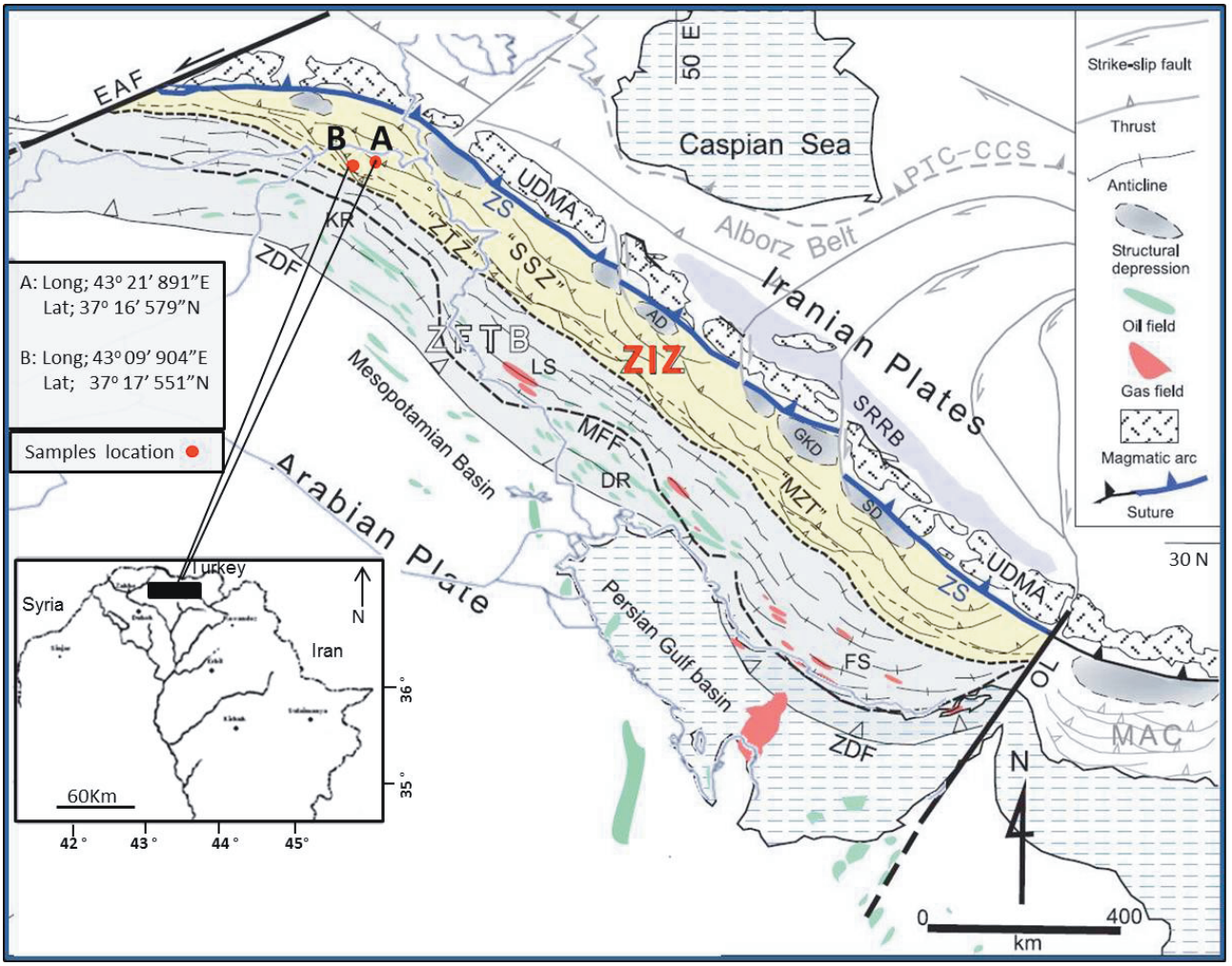

Figure 2. Subdivisions of the Zagros Orogenic Belt. AD- Arak Depression; DR- Dezful Recess; EAF- East Anatolian Fault; FS- Fars Salient; GKD- Gav Khooni Depression; KR- Karkuk Recess; LS- Lorestan Salient; MAC- Makran Accretionary Complex; MFF- Mountain Front Flexure; MZT- Main Zagros Thrust; OL- Oman Line; PTC-CCS- Paleo-Tethyan Continent-Continent Collisional Suture; SD- Sirjan Depression; SRRB- Saveh-Rafsanjan Retroforeland Basin; SSZ- Sanandaj-Sirjan Zone; ZTZ- Zagros Thrust Zone; UDMA- Urumieh-Dokhtar Magmatic Assemblage; ZDF- Zagros Deformational Front; ZFTB- Zagros Fold-Thrust Belt; ZIZ- Zagros Imbricate Zone; ZS- Zagros Suture. Hydrocarbon fields of the region, oil in green and gas in red, are shown (Alavi, 2007).

Alavi (2004, 2007), the currently two studied sections (A and B) of the Ora Formation are situated within Zagros Imbricate Zone (Figure 2).

The Hercynian orogeny was initiated in the Late Devonian and resulted in regional uplift in northern Gondwana. The Arabian plate was tilted eastward, which resulted in erosion of a thick succession of Devonian and older deposits and the development of a regional hiatus, which was called the Hercynian Unconformity or the Middle Paleozoic Hiatus (Al-Hadidy, 2007).

The Arabian plate was rotated through 90° in an anticlockwise direction and the northeastern Gondwana margin transformed from a passive to an active margin (McGillivray and Husseini, 1992). The Late Devonian-Early Carboniferous was a period of extension and compression with Hercynian back-arc rifting, inversion, and uplift. Chalki volcanics of North Iraq are formed in a back-arc setting behind the Paleo-Tethyan subduction zone (Sharland et al., 2001) (Figure 3). Although they are presently undated and could belong to Late Devonian periods (Jassim and Goff, 2006), a Hercynian age is supported by the occurrence of Devonian-Carboniferous volcanics and metamorphism found in the Sanandaj-Sirjan Zone along the southern margin of the Paleo-Tethys (Davoudzadeh and Weber-Diefenbach, 1987) (Figure 3). A geochemical investigation of Chalki rocks in northern Iraq proposed a magmatic evolution of basaltic rocks in a mafic tholeiitic suite (Ali et al., 2016).

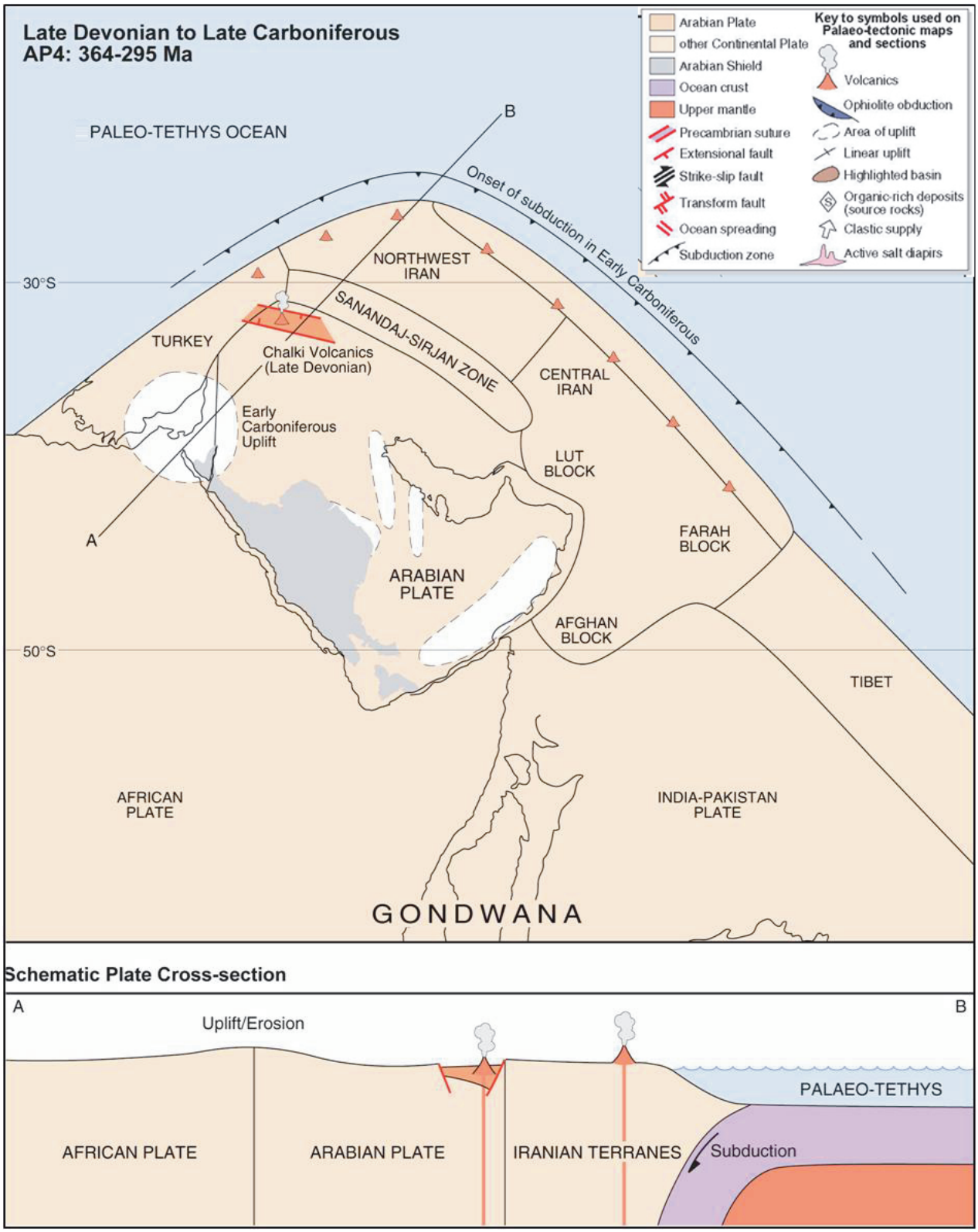

Figure 3. Schematic plate reconstruction and cross-section for megasequence AP4 (Devonian-Carboniferous) (Sharland et al., 2001).

The Paleozoic sedimentary sequences consist of three characteristic major sedimentary cycles dominated by siliciclastic or mixed siliciclastic-carbonate units (Buday, 1980; Table 1). These units are separated by major unconformities, indicating mainly the effects of the Caledonian and Hercynian Orogens. The Ordovician Khabour Formation is the oldest unit exposed in northern Iraq (Bellen et al., 1959) (Figure 1); the age is based on three *Cruziana* ichnotaxa, *Fucifera* isp., *Goldfussi* isp., and *Rugosa* isp. These three ichnotaxa are considered index fossils for the Upper Tremadocian Stage (Lower Ordovician) (Omer, 2012). In western Iraq, the Khabour Formation is overlain by the Silurian Akkas Formation, which is only known from wells; the entire Silurian and Early Devonian succession is missing in outcrop sections of northern Iraq. Here, the Khabour Formation is unconformably overlain by the Late Devonian to Early Carboniferous depositional cycle represented by the Pirispiki, Chalki, Kaista, Ora, and Harur formations (Table 1). The uppermost depositional cycle is Late Permian in age and comprises the Chia Zairi Formation (Figure 1a).

According to Jassim and Goff (2006), the upper part of the Kaista Formation is now included in the Ora Formation and the name Ora Shale has been changed to Ora Formation (Figure 1a). Behnam (2013) studied the sedimentological features of the Ora Formation and divided the Ora sequence into two units according to differences in lithology and a proposed subtidal environment for the lower part while tidal channel and intertidal flat environments were proposed for the upper part of the Ora Formation. This consists of repeated fining-upwards cycles of thin- to medium-bedded sandstones interbedded with thin-bedded shale (Figure 1b). Palynological investigation of the Paleozoic succession revealed that the Ora Formation is of Late Devonian-Early Carboniferous age (Barzinjy, 2006; Aqrawi et al., 2010).

3. Materials and methods

A total of 32 fresh samples were collected from thin- to medium-bedded sandstones of the Chalky Nasara section (37°17′551″N, 43°09′904″E), in the core of the Chiazinar fold where Paleozoic formations are successively well exposed, and 15 samples were obtained from the measured section of the Ora section (37°16′579″N, 43°21′891″E) (Figure 1b). These sections were selected because of their accessibility and good exposures. Forty-five thin sections from both sequences were polished for investigation under a standard Nikon Eclipse LV 100 POL petrographic microscope with automatic stage and petrographic examination to determine textures and mineral identification. The point-counting method of Ingersoll and Suczek (1979) was employed for quantitative compositional analysis of the framework grains (Table 2). Scanning electron microscopy (SEM) was performed using an Σ|GMA™|VP- ZEISS with EDX BRUCKER X Flash 6/10. The microscope was operated at 20 kV electron acceleration voltage, using and AsB® detector and backscattered electron (SEM-BSE) modes. X-ray diffraction analysis was performed using a Philips PW3710 diffractometer (Cu Kα radiation, 35 kV, 28.5 mA). All these studies were performed at Warsaw University, Poland.

Twenty samples were studied with hot cathode microscope HC1-LM at the Institute of Paleobiology, Polish Academy of Sciences, for visual and spectroscopic CL analyses (Neuser et al., 1996). The cathode microscope was connected to a triple-grating spectrograph of EG & G Princeton Research Instruments for recording the high-resolution spectra. The spatial resolution of spectroscopic analyses was about 30 mm. Electron energy of 14 kV and a beam current density of 0.1 μA mm^2 were used for both CL microscopy and spectroscopy.

Trace elements in quartz cement phases were analyzed by means of laser ablation inductively-coupled mass

Table 1. Three cycles of Paleozoic sedimentary sequences in Iraq by Buday (1980).

Upper Carboniferous (?)-Upper Permian Cycle	Chia Zairi Limestone with satina evaporite member
Unconformity	
Devonian (Upper Devonian)-(Lower Carboniferous) Cycle	Harur Limestone Formation Ora Shale Formation Kaista Formation
Unconformity	
Cambro-Ordovician (? Silurian)Cycle	Khabour Formation

Table 2. Modal compositions of Devonian-Carboniferous sandstones from the Ora Formation.

Cha.	Quartz						Mica			Cements						Porosity		
samp.	Qm	Qp	K	P	R.F.	Mat	Mu	Ch	Bio	Sil	Cl	Ca	Fer	HM	Pyr	PP	SP	TPC
1	54.5	5.7	2.6	1.9	3.0	1.1	5.4	3.8	1.5	11.3	3.4	0.4	0.6	1.8	1.4	0.4	1.0	364
3	59.0	6.5	0.5	1.8	0.5	1.0	1.7	2.0	0.1	16.5	3.5	0.0	0.5	3.5	0.3	0.8	2.3	318
4	51.9	5.7	1.5	1.0	5.7	1.2	4.3	2.8	2.9	9.9	5.0	1.0	1.3	1.2	1.0	0.7	2.5	322
8	53.8	6.3	1.3	1.0	5.9	1.8	2.5	2.0	1.7	11.3	5.9	0.0	1.2	1.1	1.9	0.5	1.6	303
9	54.4	5.9	3.9	1.3	1.3	1.6	2.1	1.7	2.0	9.6	5.9	0.0	1.1	1.3	2.5	1.3	3.5	394
10	56.6	7.3	2.0	1.1	1.0	1.6	2.5	1.3	2.7	11.2	4.0	0.9	2.1	1.8	1.2	1.0	1.5	341
12	59.0	4.4	1.9	0.8	0.5	1.2	2.0	1.1	0.2	16.9	5.0	0.0	0.7	3.2	0.1	2.0	1.0	389
14	55.7	6.5	3.1	0.7	0.9	1.0	1.9	1.4	1.6	12.2	5.5	0.0	1.3	2.2	1.5	1.1	2.9	322
15	57.5	4.0	2.5	0.9	0.7	0.7	1.3	0.6	1.0	15.0	5.1	0.8	1.2	2.7	1.5	1.5	2.4	391
16	60.0	6.1	1.9	0.3	0.9	0.2	1.7	0.2	0.2	15.1	5.7	0.2	1.9	2.1	0.4	0.9	2.2	312
17	59.2	5.7	1.6	0.3	1.2	1.1	1.9	0.7	1.4	13.9	5.2	0.4	1.8	2.2	0.1	1.0	1.7	397
18	60.7	4.2	1.5	1.0	0.5	1.1	1.3	1.0	1.2	16.0	4.3	0.0	1.6	2.0	0.0	2.2	0.9	304
21	62.3	6.0	1.2	0.6	0.2	0.9	2.2	1.0	1.3	14.2	4.0	0.0	1.1	1.7	1.0	2.0	0.5	356
22	59.7	5.2	1.6	0.2	1.0	0.8	2.0	0.8	1.2	15.1	5.8	0.2	1.3	1.2	1.2	1.7	1.0	331
25	58.4	5.9	1.1	0.3	0.8	0.3	1.7	0.2	0.8	18.3	5.2	0.0	0.9	1.8	0.6	0.8	2.8	357
27	60.4	6.7	1.0	0.4	0.6	0.8	1.6	1.0	1.3	14.0	4.7	0.1	1.6	2.5	0.4	1.3	1.5	337
28	61.7	6.1	1.2	0.2	0.3	0.7	1.7	0.3	0.6	14.7	5.5	0.0	1.3	2.3	0.3	1.3	1.8	355
30	60.1	4.7	1.0	0.5	0.2	1.0	1.6	1.0	1.8	16.7	5.2	0.4	1.3	1.0	0.4	1.1	2.0	340
32	62.0	5.8	0.6	0.2	0.2	0.9	2.2	1.0	1.3	14.2	4.5	0.0	0.8	2.7	1.0	0.9	2.1	359
Range	51.9–	4.0–	0.5–	0.2–	0.2–	0.2–	1.3–	0.2–	0.1–	9.6–	3.4–	0.0–	0.5–	1.0–	0.0–	0.4–	0.5–	
	62.3	7.3	3.9	1.9	5.8	1.8	5.4	3.8	2.9	18.3	5.9	1.0	2.1	3.5	2.5	2.2	3.5	
Mean	58.3	5.7	1.7	0.8	1.3	1.0	2.2	1.3	1.3	14.0	4.9	0.2	1.2	2.0	0.8	1.2	1.8	
Ora	Quartz						Mica			Cements						Porosity		
samp.	Qm	Qp	K	P	R.F.	Mat	Mu	Ch	Bio	Sil	Cl	Ca	Fer	HM	Pyr	PP	SP	TPC
2	58.5	5.7	1.1	0.2	0.3	1.1	1.7	1.0	0.9	14.3	6.3	0.3	1.3	2.9	0.9	4.0	2.1	332
3	52.2	5.9	1.5	0.3	6.9	1.4	2.3	1.9	1.5	12.2	5.7	0.0	1.9	1.3	1.6	0.6	2.9	335
4	62.6	5.6	1.4	0.2	0.9	0.4	1.1	0.5	0.2	13.8	5.9	0.2	1.8	2.2	0.5	0.9	2.2	363
7	53.0	6.3	5.6	2.0	1.3	1.0	2.0	1.8	2.0	11.4	6.2	0.0	2.4	1.8	1.0	0.4	1.8	383
8	62.0	4.7	1.0	0.4	1.0	0.8	1.6	1.0	1.8	13.6	5.2	0.4	1.3	1.4	0.4	1.1	2.0	385
9	60.9	5.4	0.9	1.0	0.5	1.0	3.2	0.9	1.1	12.6	5.1	0.8	0.9	2.0	1.0	0.6	1.8	326
11	59.3	6.3	1.1	0.9	1.0	1.6	2.3	1.2	1.7	12.6	6.8	0.2	0.0	1.3	1.3	0.8	1.5	379
13	59.5	5.9	1.8	0.3	0.9	1.1	1.9	0.7	1.4	13.9	4.3	0.6	2.0	1.6	0.0	1.5	1.7	371
14	62.4	4.3	1.5	0.3	0.7	1.0	1.6	0.8	0.9	13.2	5.7	0.0	1.6	2.4	0.4	1.3	1.9	366
15	62.1	5.8	1.2	0.6	0.7	1.1	2.3	0.6	1.1	12.8	4.9	0.0	1.8	1.4	0.3	1.3	1.6	359
Range	52.2–	4.3–	0.9–	0.2–	0.3–	0.4–	1.1–	0.5–	0.2–	11.4–	4.3–	0.0–	0.0–	1.3–	0.0–	0.4–	1.5–	
	62.6	6.3	5.6	2.0	6.9	1.6	3.2	1.9	2.0	14.3	6.8	0.8	2.4	2.9	1.6	4.0	2.9	
Mean	59.3	5.6	1.7	0.6	1.4	1.0	2.0	1.0	1.3	13.0	5.6	0.3	1.5	1.8	0.7	0.9	2.0	

Cha: Chalky Nasara section; Ora: Ora section; Samp.: Sample number; Qm: Monocrystalline quartz; Qp: Polycrystalline quartz; K: Potash feldspar; P: Plagioclase feldspar; R.F.: Rock fragment; Mat: Matrix; Mu: Muscovite; Ch: Chlorite; Si: Silica cement; Cl: Clay cement; Ca: Calcite cement; Fe: Ferruginous; HM: Heavy minerals; Pyr: Pyrite;PP: Primary porosity; SP: Secondary porosity; TPC: Total point counts.

spectroscopy (LA-ICP-MS) at the Institute of Geosciences, Goethe University, Frankfurt, Germany. The Thermo Scientific ELEMENT 2 mass-spectrometer was combined with an ArF excimer laser (Resonetics M50). Pit sizes of the laser measurements were commonly 24 μm but never exceed 32 μm because of the limited size of the quartz cements. The NIST 612 standard glass was taken as reference material whereas ^{29}Si was used for the internal standardization of the isotopes ^{7}Li, ^{11}B, ^{23}Na, ^{27}Al, ^{39}K, ^{48}Ti, ^{55}Mn, ^{57}Fe, and ^{74}Ge. A hydrothermal quartz crystal, Gig 1b (Götte et al., 2011), was measured as a mean of accuracy and reproducibility. The long-term reproducibility was about 3% and the detection limits were between 0.5 and 1.5 μmol mol^{-1} (ppt–ppb).

Microthermometric measurements on fluid inclusions were performed at Panterra Geo-Consultants in the Netherlands. Double-polished, uncovered wafers (~80–100 μm) were prepared for 3 sandstone samples of the Ora Formation. During wafer preparation, overheating was avoided and the temperature was kept below 50 °C. These wafers were initially studied with standard polarized light microscopy to identify areas with common quartz overgrowths. For the current study, an Olympus microscope with magnification range between 4× and 50× with a CCD camera attached was used. Microthermometric measurements on both primary and secondary inclusions were studied. The temperature of homogenization of vapor phase into liquid phase (Th) of aqueous inclusions was measured. Fluid inclusions were microthermometrically studied using a Linkam THMSG 600 heating-cooling stage. Calibration of the stage at 374.1 °C was performed by measuring phase changes in synthetic fluid inclusions of known composition (synthetic pure water). Reproducibility of the final melting temperature of ice (Tm_{ice}) was within ±0.2 °C and that of the homogenization temperature (Th) was within ±2 °C. CL analyses were performed on the same wafers after the standard petrography observations. CL imaging was used in order to determine with higher accuracy the target quartz cement phases. CL was carried out using a CITL Cathodoluminoscope Mk5-1. The following working conditions were used: ~18–19 kV and 350–450 μA.

4. Results

4.1. Composition of sandstones

The point-counted composition of the sandstones of the Ora Formation in the two studied sections is presented in Table 2. Quartz is the predominant detrital component and is dominated by monocrystalline quartz. The proportion of monocrystalline quartz (Qm) ranges from 51.9% to 62.3% and from 52.2% to 62.6% in the Chalky Nasara and Ora sections, respectively (Table 2). Their grain size varies between fine- to medium-grained and sorted to well-sorted, rounded to well-rounded, and less commonly subangular to angular (Figure 4a). In fine-grained sandstones it ranges from ~0.14 mm to 0.23 mm and is rounded in shape, while in medium-grained sandstones, the monocrystalline quartz ranges in size from ~0.27 mm to 0.33 mm. All types of grain contacts, including long, concave-convex, suture contacts and less commonly point contacts, are present (Figures 4b and 4c). Monocrystalline quartz grains (Qm) occur with nonundulose, slightly undulose (< 5°), and undulose (> 5°) extinction according to the terminology of Scholle (1979), Basu (1985), and Tortosa et al. (1991). Most of them show slight undulose extinction (Figure 4b). Polycrystalline quartz (Qp) is mainly composed of three or more crystals per grain, with straight to undulose extinction. Some polycrystalline quartz grains have sutured internal boundaries between composite crystals as an indication of early-stage development of metamorphic polycrystalline quartz in the source area.

Thin-bedded sandstones consist of >90% monocrystalline quartz grains and are classified as texturally supermature quartz arenites; the thick-bedded sandstones contain 84% mainly monocrystalline quartz and are texturally immature (Omer, 2015).

All studied thin sections contain lower amounts of feldspar than quartz grains. The average grain size of feldspars ranges between 0.09 mm and 0.20 mm. K-feldspar is mostly fresh (orthoclase, microcline, and microperthite; Figure 4d) and is more abundant than plagioclase in both sections, ranging in abundance from 0.5% to 3.9% in the Chalky Nasara section and from 0.9% to 5.6% in the Ora section (Table 2). It displays blue luminescence in CL, while that of rare plagioclase (albite-oligoclase) is green. Some orthoclase and plagioclase grains show alteration to kaolinite and sericite, respectively (Figure 4e). Omer (2015) suggested a multiple origin of feldspar in the sandstones of the Ora Formation as plutonic and metamorphic origin.

Lithic grains are silt-sized and mainly composed of microcrystalline aggregates of crushed muscovite, carbonate rock fragments, and less abundant metamorphic rock fragments. The average content of lithic grains is 1.3% in the Chalky Nasara and 1.4% in the Ora section.

Mica is dominated by muscovite and occasionally biotite. It is dominated by elongate muscovite flakes, which were often bucked and bent around hard detrital grains (Figure 4f). The proportion of muscovite ranges from 1.3% to 5.4% and 1.1% to 3.2% in the Chalky Nasara and Ora sections, respectively (Table 2). Random bioclasts, dominantly calcareous bivalve shells, are also noticed in these sandstones.

Heavy minerals form minor amounts (<2.5%) of the sandstones in the two studied sections. The most common is zircon, which occurs as well-rounded grains.

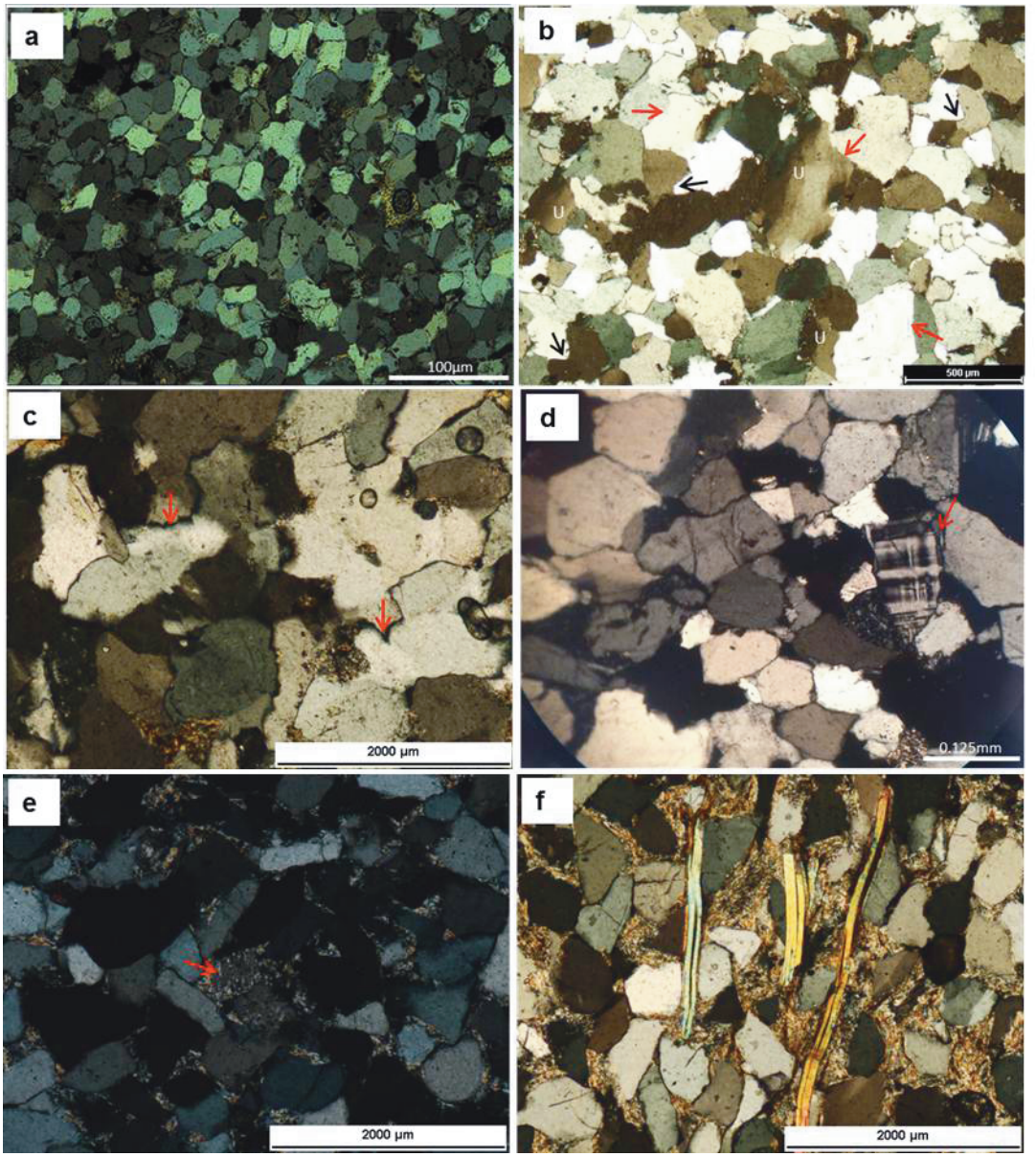

Figure 4. Photomicrographs showing framework grains in the sandstones of the Ora Formation under cross-polarized light (XPL). (a) Packed and rounded grains of monocrystalline quartz arenite sandstones with moderately open framework suggesting early, precompaction cementation. The dust-line allows the overgrowth proportion to be estimated (Chalky Nasara section, sample 3). (b) Long contact (red arrow) between monocrystalline quartz grains showing slightly undulose extinction (U) and concave-convex (black arrow) (Ora section, sample 9). (c) Compound grains with outlines of detrital quartz developed by welding of quartz overgrowth cements, forming interlocking crystalline aggregates with interpenetration texture with triple grain junctions (straight "Y" and "T" shapes). Pressure solution and suture contacts between detrital quartz grains (red arrow) (Chalky Nasara section, sample 25). (d) Microcline grain with tartan twinning and present slight overgrowths on the uppermost right margin (red arrow) (Chalky Nasara section, sample 9). (e) Early process of alteration feldspar to sericite (red arrow) (Ora section, sample 11). (f) Immature sublitharenite sandstones rich in muscovite flakes oriented and parallel to the detrital quartz grains, proof of low mechanical compaction process (Ora section, sample 3).

Other heavy minerals observed in thin sections include tourmaline, rutile, epidote, and staurolite. According to the classification of Folk et al. (1970), the sandstones of the Ora Formation are classified as supermature quartz arenite, as well as subarkose and immature sublitharenite (Omer, 2015).

4.2. Diagenetic paragenesis

The sandstones show signs of different diagenetic alterations including mechanical compaction, pressure solution, authigenic mineral formation, dissolution, and albitization of feldspars. These processes have taken place in three stages: marine eogenesis, meteoric mesogenesis, and telogenesis (Figure 5).

Quartz cement is the most important cement and makes up 9.6%–18.3% (Table 2). Three phases of quartz cement growth have been recorded by hot CL studies and the quartz cement is described in Section 4.3.

The earliest stage of paragenesis starts with both mechanical compaction and the formation of pyrite framboids in the two sections (Figure 5). The mechanical

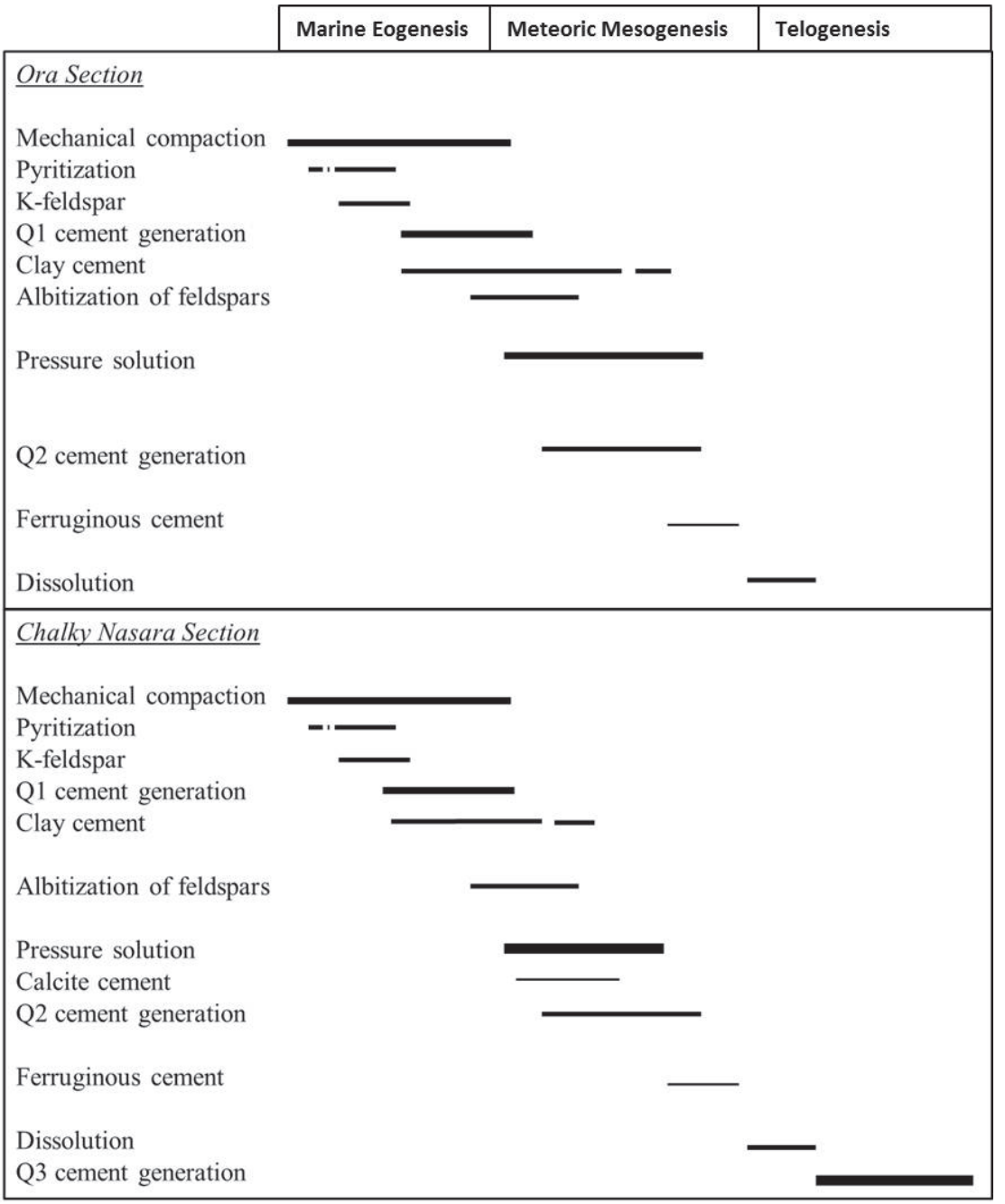

Figure 5. Sketch of the diagenetic history of the sandstones of the Ora Formation (Devonian-Carboniferous) (top: sandstones of Ora section; bottom: sandstones of Chalky Nasara section). The thickness of the lines refers to the predominant or accessory occurrences in the diagenetic minerals assemblages.

compaction is evident from the kink folds of mica minerals and disaggregation of rock fragments (Figure 6a) and the pyrite occurs in small proportions with a maximum of 2.5% (Table 2) (Figures 6b, 6c, and 6d). Calcite occurs in very small amounts (up to 1%; Table 2). The small amount is partly a result of later dissolution, and we could not estimate the ordinal amount of calcite. The dissolution of calcite contributed to the secondary porosity (up to 3.5%; Table 2). It was not possible to estimate how large a proportion of secondary porosity derived from dissolution of calcite and how much derived from dissolution of the other minerals, mainly feldspar (Figure 5). Dissolution of feldspar postdates compaction and clay cementation (Figure 6e). A small proportion of feldspar has been ablitized (Figure 5), and polysynthetic twinned plagioclases sporadically have albite overgrowths marked by lines of fluid inclusions (Omer, 2015).

The authigenic clay minerals form the second-most abundant cement in the sandstones of the Ora Formation for both sections (3.4%–6.8%). They are mainly illite and mixed-layer illite/smectite, while kaolinite constitutes a minor part in relation to the alteration of K-feldspar. The presence of illite is visible as fibrous, mat-like, and lath-shaped crystals oriented perpendicular to the grain surface and intergrown with mixed-layer illite/smectite and mud intraclasts. It occurs within quartz overgrowths in some samples, filling pores and replacing detrital grains and earlier clays, sometimes inhibiting the formation of quartz overgrowth (Figure 6f).

4.3. Cathodoluminescence petrography

4.3.1. Detrital quartz grains

Hot CL studies show that most of the detrital grains in the sandstones of the Ora Formation are monocrystalline and rounded to well-rounded in shape while the authigenically grown quartz are euhedral and rarely of bipyramidal endings filling open pore spaces (Figures 6c and 7a). Some moderately rounded grains are present in sample 22 from the Chalky Nasara section, especially in mature thin-bedded sandstones, and seldom angular grains were observed in sample 29 of the Chalky Nasara section (Figure 1b). A significant compaction caused intensive grain crushing and fragmentation/annealing of detrital grains (Figure 6c). Furthermore, pressure solution appears to have taken an important role during cementation of the sandstones (Figure 4c). Suture contacts between detrital quartz grains are only observed between grains; however, some cement has also been involved.

Changes in temperatures and pressure are a main factor controlling the CL properties of detrital quartz grains as well as the geochemistry of the depositional environment during the growth of such quartz grains and postdated geological events (Zinkernagel, 1978; Matter and Ramseyer, 1985). Quartz grains with luminescence color of brown to dark brown are the dominant grains in Ora sandstones and an indication of low-temperature metamorphic origin, while the bright blue-colored grains are of felsic magmatic and high-temperature origin (Omer, 2015) (Figures 6d and 7a–7d). The boundaries and shapes of individual quartz grains can be detected by using different CL instruments; their widths are shown in Table 3.

4.3.2. Quartz cement generations

Based on CL properties, three generations of quartz cements were observed in sandstones of the Ora Formation. The thickness of quartz overgrowths varies from one sample to another (Table 3). The first generation (Q1), which is in direct contact with quartz grains, is characterized by a thin rim and low luminescence intensity with gray to slight brown colors (Figures 6c and 7a). This type of cement is precipitated in primary pores and within mechanical cracks, reducing the intergranular porosity (Figure 7a). In some areas, the Q1 generation is volumetrically significant and postdated the onset of compaction, but it does vary and commonly has a patchy occurrence on the detrital grain surfaces with slightly brown luminescence. The Q1 cement is usually between 5 and 10 μm in thickness, but in places it has grown to larger sizes and it occasionally forms euhedral overgrowths up to 30 μm thick (Table 3). This stage is considered to be the earliest quartz cementing enveloping the margins of most of the detrital quartz grains (Figures 7a and 7b). Tiny fluid inclusions are located at the boundary between detrital grains and their overgrowths, a phenomenon documented by Friis et al. (2010). The subsequently formed quartz cement generation Q2 has a very high SEM-CL intensity, characterized by dark brown luminescing overgrowths, which are volumetrically more important in the thinly bedded sandstone than in the thickly bedded sandstones. The thickness of Q2 cement commonly ranges between 10 and 25 μm and rarely reaches up 180 μm (Table 3). It is characterized by homogeneous, strong luminescence and constitutes the final pore-filling of authigenic quartz cement, which resulted in reduction of the primary and secondary porosity, which occasionally engulfs illite (Figures 6c, 6d, 7a, and 7b). The earlier generation of illite appears to have inhibited the growth of Q2 cement within secondary pores since it predates the Q2 cementation. The remaining pore spaces were filled by the mesodiagenetic illite and Q2 type cement. Both Q1 and Q2 generations represent the common cements in the sandstones of the Ora Formation in both studied sections (Figure 5). The final quartz cementation (Q3) is observed as cryptocrystalline quartz filling in many large fractures. This is also accompanied by the filling of some chlorite sulfides. The Q3 type cement generation is characterized by darker brown luminescence and has irregular thickness ranging between 100 and 240 μm. CL images show that the previous two cement generations and the detrital quartz grains were cut by fractures filled

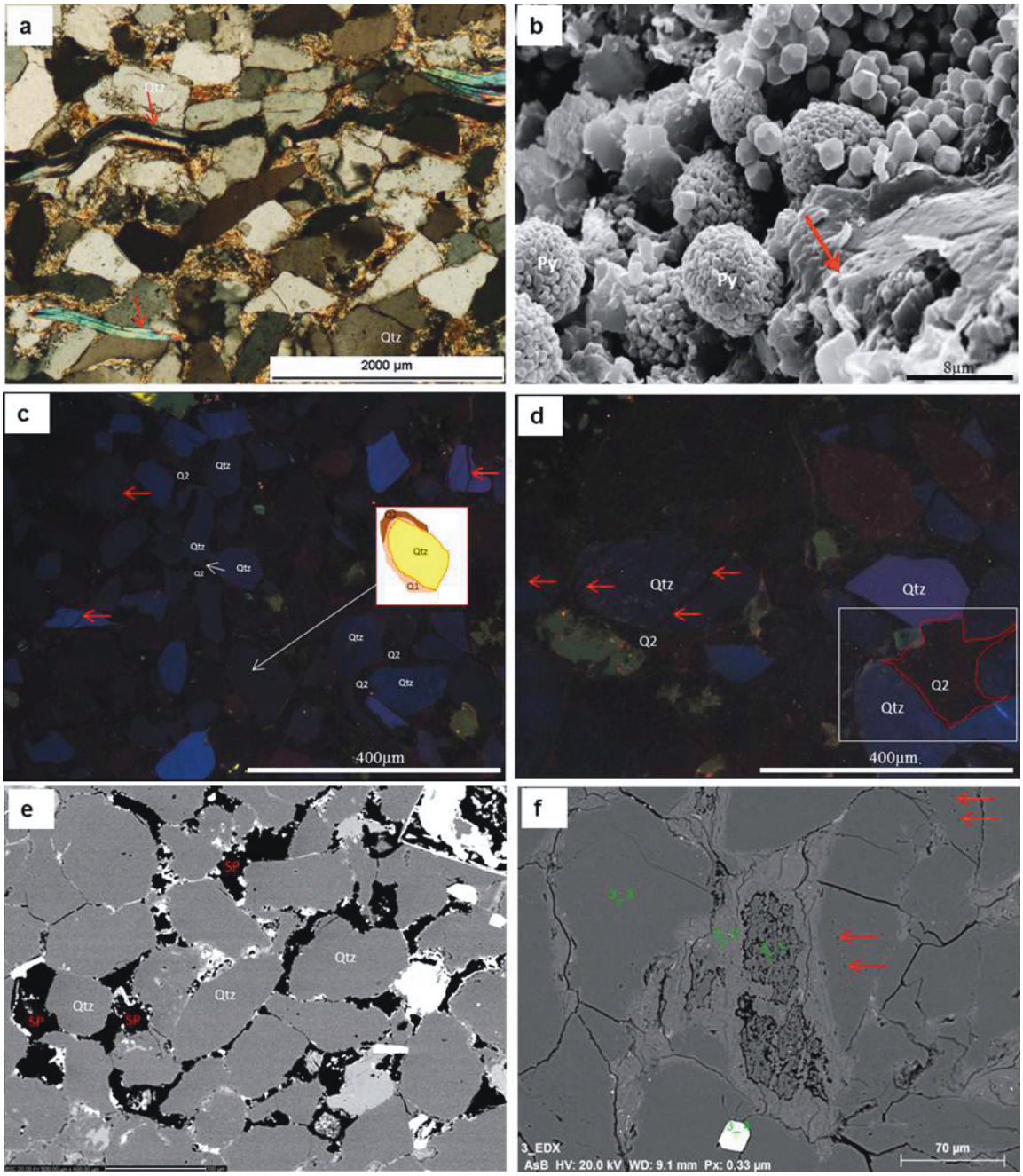

Figure 6. SEM-CL images of quartz arenite and photomicrograph of sublitharenite showing different diagenetic processes. (a) Sublitharenite sandstone pore fillings are authigenic clay, showing effects of mechanical compaction by moderate bending of muscovite (red arrow) (Chalky Nasara section, sample 4) (XPL). (b) SEM image of quartz arenite sandstone showing framboidal pyrite (Py) in pore space of sandstones and little bend of mica flakes (red arrow) of an early diagenetic process (Ora section, sample 2). (c) CL image of fine- to medium-grained quartz arenite sandstones; mechanically crushed grains are healed by cracks of detrital quartz grains (red arrow). The pore space is almost occluded by dark brown color of Q2 phase cement and thinly by slight brown color of Q1 phase cement around detrital quartz grain (white arrow) strongly cemented by quartz overgrowth cements and no intergranular porosity, thus closing primary pore spaces (Chalky Nasara section, sample 7). (d) CL image of the sandstone subjected to a second episode of crushing, affecting Q1 overgrowths (red arrow). The pervasive and common Q2 cement phase has dark brown fill of pore space (Chalky Nasara section, sample 16). (e) BSE image of feldspar dissolution and the formation of secondary porosity, thus postdating mechanical compaction and clay cement (Ora section, sample 6). (f) SEM image of quartz arenite showing authigenic illite cement located centrally between detrital quartz grains, inhibiting quartz overgrowth. K-Feldspar (3–2) alters to form illite (clay mineral), with albitization of feldspar (3–1). Detrital heavy mineral zircon setting between two quartz grains (3–4). Fluid inclusion within quartz grains that cross-cut other phases of quartz cements (red arrow) (Chalky Nasara section, sample 27). Qtz = Detrital quartz, Py = pyritization, Q1 = quartz cement generation 1, Q2 = quartz cement generation 2, SP = secondary porosity. Qtz over = Quartz overgrowth.

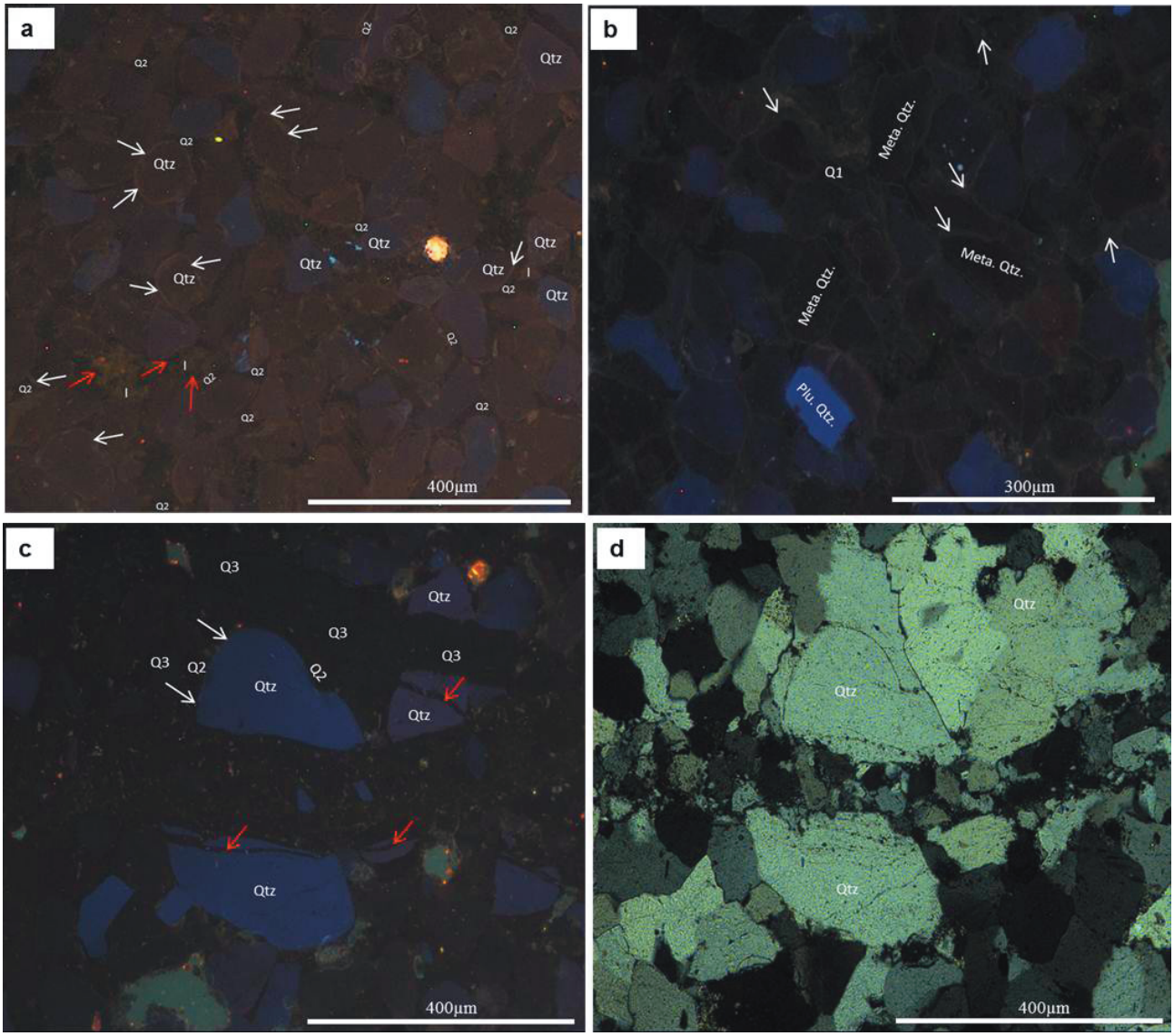

Figure 7. CL images and photomicrograph of polarizing microscope of quartz arenite sandstone showing different generations of quartz cement. (a) Thin rims of first-generation quartz cement (Q1) with slightly luminescent gray to brown color, loosely packed at margin of quartz grains, and reducing intergranular porosity (white arrow). Dark brown luminescence of second-generation quartz cement (Q2) filled secondary pores and thus engulfed authigenic illite (red arrow) (Ora section, sample 8). (b) CL image of quartz arenite sandstone, pervasive of metamorphic quartz grains, strongly cemented by quartz overgrowths of Q1 cement, luminescence and slightly brown in color (white arrow), thus reduced primary pores (intergranular porosity) (Ora section, sample 13). (c) Medium-grained sandstone was cut most by detrital quartz grains and other cements by darker brown luminescence of Q3 telogenesis stage, filling fractures, with some cracks of first crushing episode also present and indication of intensive mechanical compaction. (d) Crossed Nicols of the same view as in (c) (Chalky Nasara section, sample 22). Qtz = Detrital quartz, white arrow = Q1, red arrow = Q2, Q1 = quartz generation cement 1, Q2 = quartz generation cement 2, Q3 = quartz generation cement 3, I = authigenic illite, Plu = plutonic quartz, Meta = metamorphic quartz.

by Q3 type cement (Figure 7c) Q3 type cementation is restricted to the sandstones of the Chalky Nasara section. Illite also accompanies the Q3 cement generation, which initially shows a low and weak luminesce that change into brownish colors.

The identification of the Q2 and Q3 cement generations is basically impossible with optical microscopy alone (Figures 7c and 7d). Cases similar to that of Q3 cement have been described by others (e.g., Milliken and Laubach, 2000; Friis et al., 2010; Omer and Friis, 2014).

Table 3. Widths of detrital quartz grains and quartz generation cements from the sandstones of the Ora Formation, North Thrust Fault, examined under hot CL.

Sample	Grain size (μm)		Quartz cements width (μm)	
	Minimum	Maximum	Minimum	Maximum
Ch. 4	75	180	Q1, 3	Q1, 7
			Q2, 10	Q2, 17
			Q3, 110	Q3, 190
Or. 5	90	200	Q1, 5	Q1, 9
			Q2, 14	Q2, 24
Or. 8	85	190	Q1, 7	Q1, 10
			Q2, 12	Q2, 20
Ch. 6	80	210	Q1, 4	Q1, 10
			Q2, 50	Q2, 190
Ch. 20	55	110	Q1, 10	Q1, 30
			Q2, 25	Q2, 50
Ch. 28	100	250	Q1, 5	Q1, 10
			Q2, 10	Q2, 20
			Q3, 100	Q3, 240

Ch.: Chalky Nasara section; Or.: Ora section; Q1: Quartz generation cement 1; Q2: Quartz generation cement 2; Q3: Quartz generation cement 3.

4.4. Trace element geochemistry of quartz cements

Trace element CL profiles were determined across the detrital quartz and quartz cements (Figures 6c, 6d, and 7c) and the results of trace element analyses of three types of quartz cements and detrital quartz grains are summarized in Table 4. The trace element compositions of quartz overgrowths in the Ora sandstones are very similar to those reported for other low-temperature authigenic and hydrothermal quartzes (Rusk et al., 2008; Friis et al., 2010; Götte et al., 2011, 2013; Lehmann et al., 2011).

The trace element compositions of quartz cements in the Ora Formation sandstones are dominated by Al, K, Li, and Fe. The concentrations of these elements vary strongly and the main differences between detrital quartz and quartz cements are shown in their Li and Al contents. Aluminum content shows a much larger variation (up to 39000 ppm) in the first generation (Q1) of quartz cement in the Chalky Nasara section than in the detrital quartz (up to 7500 ppm; Table 4). Li content also shows lower concentrations in the detrital quartz than in the Q1 cement (up to 70 ppm) in the Chalky Nasara section. The same phenomena were described by Demars et al. (1996) in quartz overgrowths in the Paris Basin Keuper sandstones.

A bright luminescence with a slightly brownish color is the main feature to distinguish Q1 type cement from the others (Figures 7a and 7b). Significant positive correlation of Al with Li has been found in the Q1, Q2, and Q3 cement generations and detrital quartz in the Ora section with average correlations (R) of 0.906, 0.832, 0.915, and 0.934, respectively. However, the same elements in the detrital quartz grains in the Chalky Nasara section do not show any correlation. The distribution of Al and Li shows different patterns among samples from the two Ora sandstones (Figures 8a–8d). Al, Li, and H have been found as the most important in authigenic hydrothermal and metamorphic quartz (Götte and Ramseyer, 2012).

Germanium is found in low concentrations in both quartz cements and detrital quartz, ranging between 0.39 and 6.80 ppm in overgrowth cements and 0.4 and 3.24 ppm in detrital quartz grains (Table 4). There is a significant positive correlation between Ge and Al in the Q3 cement (R = 0.899) and quartz grains (R = 0.743) in the Ora section, while those in the Chalky Nasara section are weak (R = 0.475) (Figures 9a–9c). Germanium is also positively correlated with Fe (R = 0.894) in the Q3 cement (Figure 9d).

Sodium shows a strong positive correlation with Al in all Q2 quartz cements (R = 0.934) and detrital quartz (R = 0.921) in the Ora section (Figure 9e), which is not the case for Q3 cement in the Chalky Nasara section, which could be the result of ablation of aqueous high-salinity microinclusions within the authigenic quartz during

Table 4. Results of trace element analyses for the sandstones of the Ora Formation measured by LA-ICP-MS.

Analysis no.	Li_{ppm}	B_{ppm}	Na_{ppm}	Al_{ppm}	K_{ppm}	Ti_{ppm}	Mn_{ppm}	Fe_{ppm}	Ge_{ppm}	Li/Al
	Ora section - sandstone, quartz cement 1									
1	1.01	1.50	4.03	196.78	758.21	2.65	1.00	514.28	1.17	0.01
2	7.82	1.89	131.89	4228.11	2055.72	2.18	n.d.	8923.50	0.67	0.00
3	2.60	1.06	28.23	242.61	93.39	n.d.	1.54	131.47	1.07	0.01
4	3.20	n.d.	3.66	179.73	14.33	0.76	2.20	1938.13	0.98	0.02
5	2.17	n.d.	19.52	1321.03	338.63	5.77	2.21	1365.10	0.75	0.00
6	26.28	n.d.	207.17	25290.17	7347.78	4.66	n.d.	39099.90	1.59	0.00
7	0.32	n.d.	13.95	1786.62	698.97	n.d.	n.d.	318.54	0.65	0.00
8	1.27	0.88	23.51	359.74	83.35	4.62	0.48	212.41	1.58	0.00
9	0.35	0.80	3.82	18.42	7.65	2.35	0.43	143.92	0.61	0.02
10	1.16	0.89	12.60	40.53	4.51	1.49	0.33	69.48	0.59	0.03
11	4.93	n.d.	66.83	10556.84	4710.08	2.42	1.73	3870.90	1.80	0.00
12	0.83	n.d.	15.68	2302.46	1022.05	n.d.	0.71	762.52	1.12	0.00
13	0.67	n.d.	75.41	1303.14	n.d.	8.25	1.82	1140.10	1.25	0.00
14	1.68	n.d.	8.04	34.35	11.51	1.57	0.85	193.59	1.20	0.05
15	6.29	1.68	12.90	239.40	77.03	3.19	0.71	214.44	1.01	0.03
16	9.17	n.d.	1207.40	20376.11	102805.00	n.d.	n.d.	10566.00	2.41	0.00
17	23.16	n.d.	9.75	1090.86	385.56	0.94	0.51	117.77	1.88	0.02
18	37.05	0.08	13.67	6439.26	369.19	1.32	n.d.	19809.30	1.74	0.01
19	10.62	n.d.	59.82	4543.39	2070.64	1.44	n.d.	1964.00	1.98	0.00
20	34.56	n.d.	74.64	757.56	107.21	3.02	n.d.	2100.10	1.49	0.05
21	3.08	n.d.	15.69	77.48	8.04	1.26	0.71	160.70	0.85	0.04
22	1.66	n.d.	31.60	703.55	278.61	n.d.	1.55	230.74	1.18	0.00
23	1.46	0.76	3.50	63.89	n.d.	n.d.	0.28	71.27	0.97	0.02
Average	7.54	1.06	85.13	3571.83	5868.94	2.82	1.06	3913.30	1.24	0.01
	Chalky Nasara section - sandstone, quartz cement 1									
24	6.89	n.d.	62.42	8619.39	4535.17	n.d.	2.01	11613.90	2.16	0.00
25	0.19	0.59	2.73	8.55	3.86	2.82	0.25	64.45	0.57	0.02
26	11.23	n.d.	13.76	2030.85	907.81	4.97	1.71	2152.00	1.95	0.01
27	41.18	n.d.	118.80	17515.07	6074.14	n.d.	n.d.	37556.00	3.21	0.00
28	1.98	1.63	6.82	417.69	89.33	n.d.	0.67	1017.10	0.99	0.00
29	24.30	n.d.	7.93	410.63	11.81	1.63	0.78	196.12	1.96	0.06
30	73.06	n.d.	301.52	39824.30	9056.20	n.d.	n.d.	111037.00	2.74	0.00
31	20.29	n.d.	68.85	5796.74	1614.52	6.25	n.d.	19296.00	1.55	0.00
32	22.58	1.62	7.00	713.74	46.84	n.d.	1.30	948.37	2.23	0.03
33	20.56	n.d.	493.48	9497.72	13448.32	n.d.	n.d.	241497.00	2.29	0.00
34	5.26	n.d.	16.35	646.79	198.86	n.d.	1.66	2155.70	1.03	0.01
35	1.89	1.35	5.68	22.22	8.68	3.58	0.60	346.31	0.83	0.09
Average	19.00	1.29	92.08	7125.31	2999.66	3.85	1.28	35656.60	1.79	0.02

Table 4. (Continued).

	Ora section - sandstone, quartz cement 2									
36	6.21	0.84	34.51	452.75	77.67	1.73	1.32	522.38	1.34	0.01
37	5.66	n.d.	13.85	456.76	5.03	2.01	1.42	1026.20	1.39	0.01
38	6.29	0.66	3.56	97.18	4.77	0.57	0.38	102.46	1.74	0.06
39	1.07	0.71	38.47	20.36	4.81	1.06	0.68	107.99	0.58	0.05
40	14.25	0.79	28.35	269.00	5.00	0.62	1.89	114.55	1.88	0.05
41	3.23	n.d.	18.83	705.53	160.66	n.d.	1.41	1865.50	0.81	0.00
42	22.25	n.d.	505.39	25206.09	9459.06	n.d.	n.d.	39271.10	0.80	0.00
43	10.29	0.79	3.74	201.44	5.11	0.68	0.41	15.16	2.00	0.05
44	0.31	0.79	4.72	11.03	4.45	3.76	0.30	73.48	0.61	0.03
45	16.29	n.d.	516.12	14201.41	6159.46	2.06	0.86	206.12	1.21	0.00
46	2.98	n.d.	34.63	1381.62	605.33	n.d.	n.d.	4888.60	0.68	0.00
47	3.48	1.58	163.52	1734.16	649.19	n.d.	2.07	3719.20	0.86	0.00
48	0.49	n.d.	7.05	26.17	10.67	8.06	0.72	178.46	1.00	0.02
49	16.29	n.d.	516.12	14201.41	n.d.	2.06	0.86	206.12	1.21	0.00
50	3.41	1.55	34.01	1700.00	650.30	n.d.	3.10	4698.00	0.77	0.00
Average	7.53	0.96	128.20	4044.33	1271.54	2.26	0.95	3799.70	1.13	0.02
	Chalky Nasara section - sandstone, quartz cement 3									
51	2.50	0.64	56.26	177.61	65.48	8.43	0.78	95.25	1.46	0.01
52	4.33	1.01	16.41	499.97	126.56	4.63	1.63	251.87	0.47	0.01
53	1.35	0.72	40.78	155.46	37.01	2.49	0.48	98.75	1.24	0.01
54	2.77	n.d.	20.02	1444.51	n.d.	7.15	1.14	636.18	0.73	0.00
55	3.76	n.d.	42.69	662.57	221.35	n.d.	0.56	147.06	0.56	0.01
56	8.10	n.d.	17.83	1278.46	224.27	n.d.	0.14	2337.03	1.58	0.01
57	3.88	0.79	47.01	1071.51	365.00	4.64	0.48	379.07	0.93	0.00
58	1.10	1.31	4.05	84.16	53.60	9.46	0.83	88.24	0.68	0.01
59	10.70	1.88	8.69	3490.51	639.30	7.01	n.d.	11022.40	1.27	0.00
60	10.92	n.d.	n.d.	1068.30	186.59	2.55	n.d.	5786.90	0.57	0.01
61	0.87	1.66	2.61	797.96	246.89	5.08	2.42	3035.60	0.39	0.00
62	3.97	n.d.	39.72	811.26	271.35	1.38	1.18	1482.10	0.88	0.00
63	3.02	1.08	7.45	2227.77	614.16	n.d.	2.63	4982.70	0.49	0.00
64	1.64	n.d.	3.17	197.11	14.21	1.05	n.d.	2369.40	1.72	0.01
65	5.77	0.87	5.89	209.38	5.34	n.d.	0.85	452.54	1.22	0.03
66	16.16	1.47	14.54	1909.87	404.48	7.22	4.51	4925.95	1.60	0.01
67	2.12	n.d.	12.38	263.58	93.29	n.d.	0.26	116.88	1.60	0.01
68	50.44	n.d.	46.60	23810.71	n.d.	n.d.	n.d.	50361.00	6.80	0.00
69	3.26	n.d.	n.d.	1688.29	625.15	n.d.	n.d.	5962.50	2.37	0.00
70	14.99	0.65	n.d.	610.74	72.27	n.d.	1.02	1073.30	2.20	0.02
71	12.17	0.78	36.95	309.42	34.60	4.05	0.47	349.51	0.96	0.04
Average	8.03	1.07	23.73	2036.63	226.36	5.01	1.19	4569.20	1.41	0.00

Table 4. (Continued).

	Ora section - sandstone, quartz grains									
72	0.63	0.77	3.55	16.82	4.82	2.54	n.d.	126.05	0.63	0.04
73	0.53	0.78	44.35	17.07	7.60	9.60	2.01	330.97	0.58	0.03
74	1.39	n.d.	31.25	19.62	5.43	4.23	1.30	155.00	0.66	0.07
75	0.35	n.d.	3.50	30.66	4.71	2.41	2.08	203.34	1.40	0.01
76	0.48	0.92	3.85	20.87	6.12	1.80	0.38	79.76	0.54	0.02
77	14.07	0.80	10.56	241.58	4.34	0.74	0.31	66.97	1.57	0.06
78	0.22	n.d.	3.93	11.30	3.94	1.32	0.67	62.64	0.41	0.02
79	1.04	n.d.	12.80	144.60	38.88	4.80	0.31	246.29	0.67	0.01
80	0.23	0.82	3.02	269.33	130.01	2.08	0.57	439.89	0.50	0.00
81	0.55	1.82	29.61	459.35	192.46	3.79	0.41	171.25	1.25	0.00
82	3.44	n.d.	7.37	96.78	10.62	n.d.	0.83	185.03	1.18	0.04
83	0.90	0.90	10.18	14.62	4.52	2.74	1.47	82.55	0.73	0.06
84	44.59	n.d.	161.56	3940.57	13532.58	n.d.	n.d.	51451.00	2.38	0.01
85	32.11	n.d.	37.12	1571.99	245.79	5.67	0.83	181.57	0.96	0.02
86	0.22	0.74	10.67	15.60	3.18	6.54	0.26	63.80	0.94	0.01
87	0.57	n.d.	31.79	85.56	40.04	4.21	0.75	301.82	0.56	0.01
Average	6.31	0.94	25.32	437.77	889.68	3.75	0.82	3384.30	0.94	0.03
	Chalky Nasara section - sandstone, quartz grains									
88	10.65	n.d.	7.78	565.56	174.58	n.d.	0.23	n.d.	1.58	0.02
89	0.34	0.76	4.90	11.35	15.16	3.31	0.13	n.d.	0.48	0.03
90	12.83	n.d.	30.26	1357.69	439.34	n.d.	1.07	380159.00	0.95	0.01
91	1.01	n.d.	14.46	26.89	n.d.	1.26	0.53	3011.30	1.16	0.04
92	44.30	n.d.	104.00	1456.97	7455.78	n.d.	n.d.	34098.00	1.94	0.03
93	2.27	1.62	9.18	227.05	78.48	n.d.	0.47	932.69	1.51	0.01
94	10.89	n.d.	9.35	3124.16	937.23	n.d.	1.30	3847.20	1.37	0.00
95	10.76	1.58	43.96	1141.94	385.22	0.19	2.02	1524.70	0.71	0.01
96	2.66	n.d.	60.01	839.57	346.17	n.d.	2.18	3235.50	0.81	0.00
97	1.14	1.92	29.95	54.43	24.52	4.01	n.d.	2015.70	1.84	0.02
98	15.83	n.d.	198.03	5973.65	24306.72	n.d.	n.d.	4200.50	1.72	0.00
99	0.79	n.d.	30.56	7276.64	3032.91	n.d.	1.98	11634.70	3.24	0.00
100	45.61	n.d.	131.85	2163.54	2864.24	2.85	n.d.	76640.00	1.45	0.02
101	7.33	1.35	4.82	1152.22	198.24	n.d.	2.10	2054.40	1.65	0.01
102	0.87	1.90	8.08	353.64	102.88	0.59	0.80	512.17	1.17	0.00
103	15.60	n.d.	173.69	3389.13	7689.18	n.d.	n.d.	75670.00	2.32	0.00
104	1.16	0.61	2.64	16.11	4.05	n.d.	0.60	66.54	0.85	0.07
105	0.54	1.05	8.07	62.16	33.02	1.36	0.80	198.74	1.58	0.01
106	3.26	1.01	7.38	92.88	15.70	2.43	2.09	181.42	1.09	0.04
Average	9.88	1.31	46.26	1541.35	2672.41	2.00	1.16	31578.00	1.44	0.02

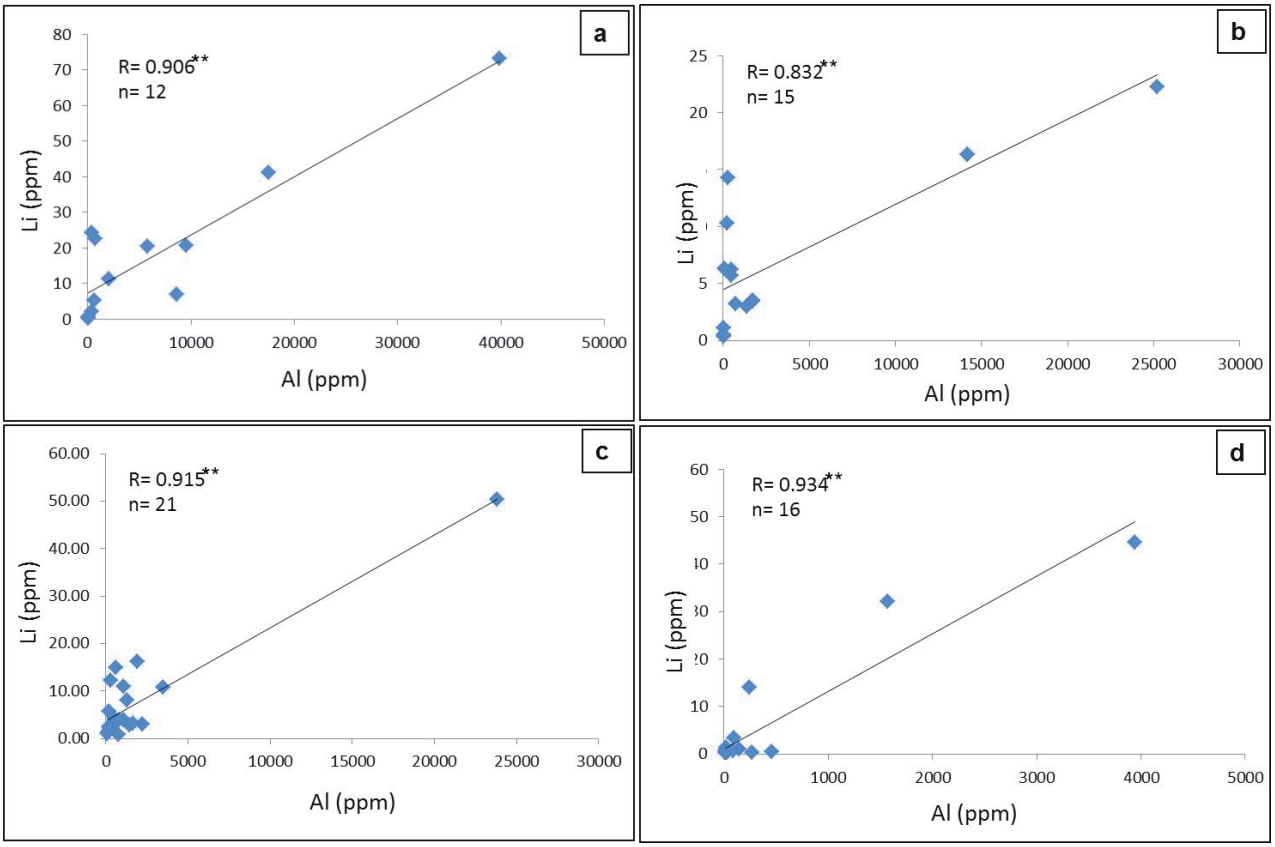

Figure 8. Relationships between trace elements Al and Li in the sandstones of Ora Formation measured by LA-ICP-MS. (a) A positive correlation coefficient between Li and Al in quartz overgrowth cement (Q1) in Chalky Nasara section. (b) Quartz overgrowth cement (Q2) in Ora section. (c) Quartz overgrowth cement (Q3) in Chalky Nasara section. (d) A positive correlation coefficient as indicated by plotted Li versus Al in detrital quartz grains in Ora section.

LA-ICP-MS measurement (Hartmann et al., 2000b). Potassium content of some detrital quartz grains is higher than that of Na. Such characteristics have previously been observed in agates where K is incorporated with Al as a charge-compensating cation (Merino et al., 1995). A strong correlation between Al and K is observed in Q3 cement (R = 0.828; Figure 9f). The distributions of the other analyzed elements (Ti, Mn, and B) do not show any systematic differences between the quartz overgrowths and detrital quartz grains in the Ora sandstones. However, the average Ti contents in Q3 cement and detrital quartz in the Ora section are up to 5.01 ppm and 3.75 ppm, respectively. Higher Ti concentrations were observed by Van den Kerhof et al. (1996), proposed to be due to quartz derived from granulites. In the current study Ti concentrations are lower in quartz cements and refer to hydrothermal origin (Müller et al., 2003).

4.5. Fluid inclusion measurements of quartz cements

The microthermometric measurements of fluid inclusions in quartz overgrowth cements are given in Table 5. Synthetic fluid inclusion samples provided by the Linkam stage manufacturers were used to calibrate the stage before the measurements of homogenization temperatures of the studied samples. This standard contains fluid inclusions with pure water (wt. 0% salinity). At room temperature the inclusions are liquid/vapor two-phased inclusions; heating them up to 374.1 °C (pure water critical point) verifies that the stage is working properly.

On the basis of petrography and CL observations, each of the fluid inclusions was assigned to different quartz cement generations: Q1, Q2, and Q3. Three sandstone samples were examined for their fluid inclusion contents. Their sample numbers are 16 and 22 from the Chalky Nasara section and 14 from the Ora section (Figure 1b).

Petrographically, the examined samples of the Chalky Nasara section are fine- to medium-grained, subrounded to rounded, well-sorted sandstones with rare ductile clay grains, clay matrix, and heavy minerals. The fluid inclusions of three quartz cement generations were identified. The fluid inclusions entrapped by the quartz overgrowths are rare, elongated to rounded, two-phased (L/V), and liquid-dominant at room temperature and inclusions are

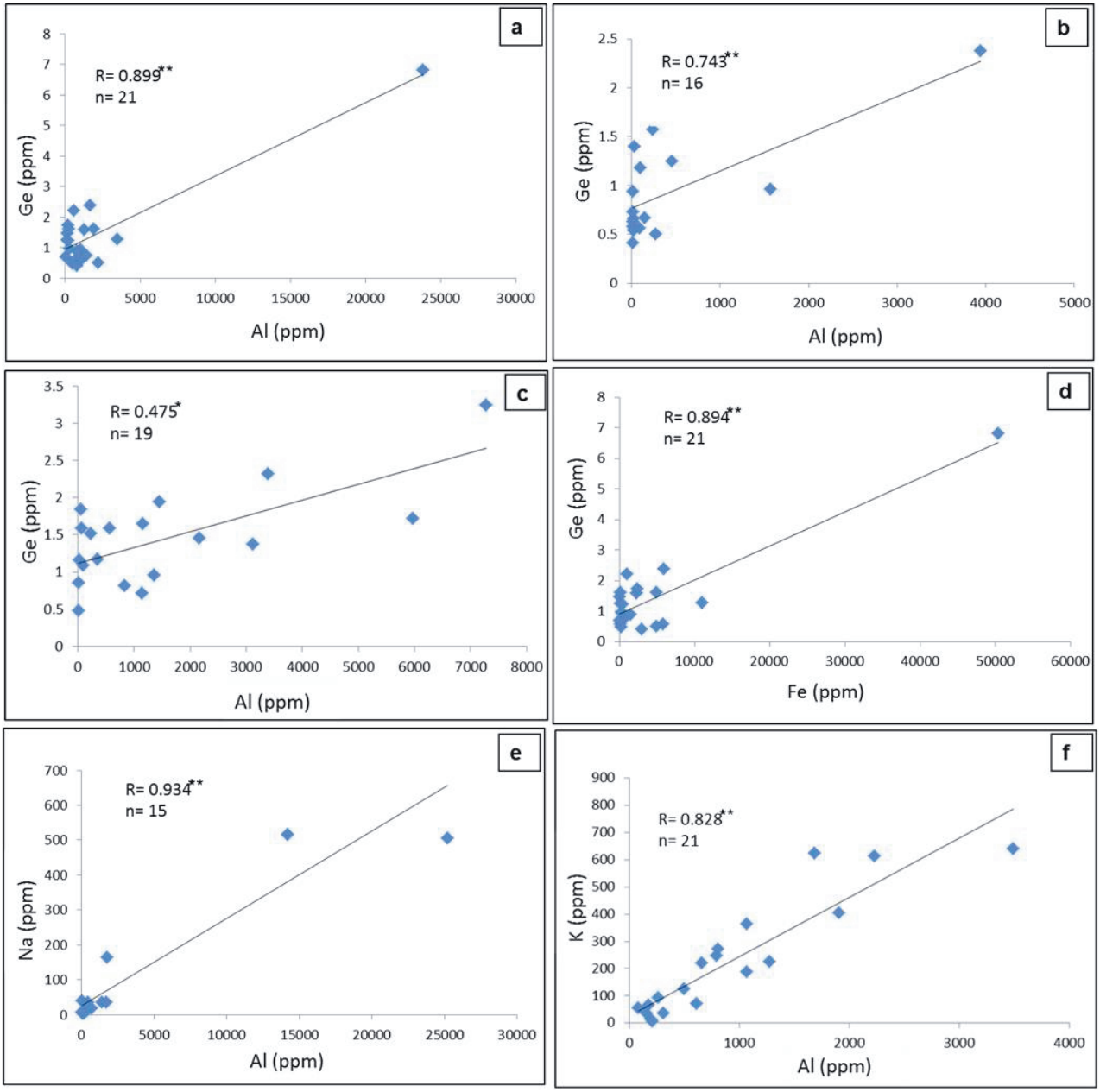

Figure 9. Relationships of trace elements in the sandstones of Ora Formation. (a, b, c) Positive correlations between Al and Ge are found in quartz cement generation Q3 and detrital quartz grains in Ora and Chalky Nasara sections, respectively. (d) A strong positive correlation between Ge and Fe in Q3 Chalky Nasara section. (e) A positive correlation between Al and Na in Q2 cement Ora section. (f) A positive correlation between Al and K in Q3 cement Chalky Nasara section.

about 5–15 μm in size. Twenty-two microthermometric measurements were performed on Chalky Nasara samples and six on Ora samples (Table 5). Homogenization temperatures (Th) of the fluid inclusions in the Chalky Nasara section of the first-generation quartz cements (Q1) reveal primary inclusions with a homogenization temperature ranging between 154.5 and 160.0 °C. The fluid inclusions of the second generation of quartz cements (Q2), which show dark brown luminescence overgrowths (Figure 6d), are also primary, with a Th ranging between 160.0 and 165.5 °C (Table 5). The fluid inclusions within the Q3 cement are of secondary origins and have a characteristic white-blue fluorescence under the ultraviolent light and a yellow color under blue light. They cross-cut other cements and quartz grains and have a Th ranging between 167.5 and 177.5 °C (Figures 7c, 10a,

Table 5. Microthermometry results of the quartz cement generations in representative samples from the Ora Formation.

Sample no.	Fluid no.	Host mineral	Type fluid	Qtz. cem. gen.	Fluid phase	Fluid shape	V/L ratio	Th (°C) Lv to L	Tm ice (°C)	Salinity (mass %)
				Chalky Nasara section						
16	1	Quartz overgrowth	Primary	1	V/L	Rectangular	0.25	155.5	–2.20	3.70
	2	Quartz overgrowth	Primary	1	V/L	Rectangular	0.25	157.5	–2.00	3.30
	3	Quartz overgrowth	Primary	1	V/L	Rounded	0.25	156.0	–1.70	2.90
	4	Quartz overgrowth	Primary	1	V/L	Elongated	0.20	160.0	–1.80	3.00
	5	Quartz overgrowth	Primary	2	V/L	Elongated	0.17	163.0	–1.80	3.00
	6	Quartz overgrowth	Primary	2	V/L	Irregular	0.22	165.5	–2.00	3.30
	7	Quartz trail/vein	Secondary	3	V/L	Irregular	0.22	167.5	–3.59	6.10
	8	Quartz trail/vein	Secondary	3	V/L	Rounded	0.18	176.5	–3.00	5.00
	9	Quartz trail/vein	Secondary	3	V/L	Rounded	0.19	177.0	–3.24	5.40
	10	Quartz trail/vein	Secondary	3	V/L	Rounded	0.22	177.5	–3.03	5.05
	11	Quartz trail/vein	Secondary	3	V/L	Elongated	0.17	176.5	–3.48	5.80
	12	Quartz trail/vein	Secondary	3	V/L	Rounded	0.18	177.0	–3.84	6.40
	13	Quartz trail/vein	Secondary	3	V/L	Elongated	0.30	169.0	–3.00	5.00
	14	Quartz trail/vein	Secondary	3	V/L	Irregular	0.10	176.5	–3.42	5.70
	15	Quartz trail/vein	Secondary	3	V/L	Rounded	0.30	169.0	–3.54	5.90
	16	Detrital quartz	Primary	-	V/L	Irregular	0.15	194.0	-	-
22	17	Quartz overgrowth	Primary	1	V/L	Irregular/elongated	0.30	155.0	–2.10	3.55
	18	Quartz overgrowth	Primary	1	V/L	Irregular/elongated	0.25	156.0	–2.00	3.30
	19	Quartz overgrowth	Primary	1	V/L	Irregular/elongated	0.20	156.5	–2.30	3.87
	20	Quartz overgrowth	Primary	1	V/L	Elongated	0.25	160.0	–1.90	3.25
	21	Quartz overgrowth	Primary	2	V/L	Irregular	0.27	161.5	–2.20	3.70
	22	Quartz trail/vein	Secondary	3	V/L	Rounded	0.18	177.0	–3.09	5.20
	23	Quartz trail/vein	Secondary	3	V/L	Rounded	0.25	170.5	–3.42	5.70
	24	Detrital quartz	Primary	-	V/L	Elongated	0.20	203.0	-	-
				Ora section						
14	25	Quartz overgrowth	Primary	1	V/L	Irregular	0.22	154.5	–2.30	3.90
	26	Quartz overgrowth	Primary	1	V/L	Irregular/elongated	0.20	156.5	–2.20	3.70
	27	Quartz overgrowth	Primary	1	V/L	Elongated	0.25	158.5	–2.20	3.70
	28	Quartz overgrowth	Primary	2	V/L	Irregular	0.33	162.5	–2.00	3.30
	29	Quartz overgrowth	Primary	2	V/L	Rounded	0.33	160.0	–1.80	3.30
	30	Quartz overgrowth	Primary	2	V/L	Rounded	0.33	163.5	–1.70	2.90
	31	Detrital quartz	Primary	-	V/L	Irregular	0.27	198.5	-	-

Th: Temperature of homogenization; V: Vapor; L: Liquid; Tm: Temperature of melting ice.

10b, 11a, and 11b). The Th for the primary fluid inclusions in detrital quartz grains ranges between 194 °C and 203 °C. The higher homogenization temperature of inclusions in the detrital grain shows different temperature regimes, probably because of their metamorphic or magmatic origins.

Six microthermometric measurements were carried out for sample 14 of the Ora section (Figures 10c, 10d, and 11c). This sample is very fine-grained, subangular, and moderately sorted with significant clay laminae. Q1 and Q2 type quartz overgrowths are found as irregular rims around detrital quartz grain and as filling secondary pores, respectively. The range of homogenization temperatures of primary fluid inclusions in the Q1 and the dark brown luminescent Q2 quartz cements are 154.5–158.5 °C and 160.0–163.5 °C, respectively (Figures 10c and 10d). The Th for the fluid inclusions in the detrital quartz of this sample is 198.5 °C (Table 5).

5. Discussion

5.1. Diagenetic history

Except for cases where detrital clay forms the matrix, textural parameters do not seem to have played an important role on the distribution of quartz cements in the sandstones of the Ora Formation. The thin interlaminated shale layers within the thinly bedded sandstones are considered to be the main source of quartz cements in these sandstones. This is supported by the high concentrations of clay-compatible trace elements in the quartz cement. Thus, depositional facies have played an indirect controlling role on the distribution of the three quartz cement generations by the facies control on the content of detrital matrix. The sandstones of the Ora Formation from the two studied sections were subjected to quartz cement generation in three episodes. These are the episodes of marine eogenesis, meteoric mesogenesis, and telogenesis (Figure 5). The main diagenetic stages observed in the Ora sandstones are (1) mechanical and chemical compaction; (2) authigenic clay; (3) quartz cement generation in three episodes; (4) formation of calcite cement; (5) dissolution of calcite and feldspar; and (6) albitization of feldspar (Figure 5). The earliest stage of eogenesis is the formation of pyrite framboids, which are related to the local conditions of the sulfide concentration formed by sulfate-reducing bacteria being higher than the concentration of available ferrous iron (Postma, 1982); this stage was observed in the two sections of the Ora sandstones (Figure 5). Furthermore, mechanical compaction took place in the eogenesis stage, which is evident from the bending of mica flakes and tighter packing of detrital grains. The eogenetic compaction caused a significant reduction of primary porosity (Figures 4a and 6a). The effect of compaction is also evident from the concave-convex suture contacts of neighboring quartz grains (Figure 4c). Mechanical compaction is also partly caused by intense grain fracturing (Figures 6c and 6d), which also affected the Q1 and Q2 cement generations. Brittle deformation is a common feature of the studied Devonian-Carboniferous sandstones and significantly contributed to compaction (Figures 6c, 6d, and 7c). When associated with the total annealing of crushed grains, brittle deformation cannot be distinguished without the aid of SEM-CL studies (Dickinson and Milliken, 1995; Makowitz and Milliken, 2003). Because the brittle deformation also affected the Q1 and Q2 cement generations, it must have occurred late in the mesogenesis stage or in the telogenesis stage. Therefore, it may have been caused by the high stress level associated with tectonic thrusting and uplift.

The chemical compaction occurred by pressure solution along both intergranular contacts and fractures during meteoric mesogenesis (Zhang et al., 2008). Textural traces of this compaction can be observed along detrital grains and more evidently along the pervasive microstylolites produced by pressure solution. Microstylolite is a ubiquitous feature of the supermature sandstones of the Ora Formation and has taken place prior to any significant cementation (Figure 4c). However, the pressure solution is known to start at grain contacts as a result of gradually increasing stress, which generally originated from increasing load pressure during advancing burial of siliciclastic sediments (Sibley and Blatt, 1976; Tada and Sieve, 1989; Dutton and Diggs, 1990). As a consequence, accumulation of dissolved quartz in intergranular pores under lower pressures relative to those along the grain contacts reduces porosity (Angevine and Turcotte, 1983). This phenomenon is a common feature in the sandstones of Chalky Nasara section (Figures 4c and 10a).

As a paragenetic mineral, calcite cementation played a significant role in reducing the porosity of sandstones from the Chalky Nasara section. During the meteoric mesogenesis stage, authigenic illite and minor amounts of mixed layer illite/smectite formed as grain coats on detrital grains or as pore-filling cement and occluded primary porosity and inhibited quartz overgrowths (Figures 6f and 7a). Illite, which typically forms during a progressive burial stage at temperatures of 90–130 °C (Morad et al., 2000), requires K-rich pore water. Mixed-layer illite/smectite is also observed as pore-lining to pore-filling and having ragged-platy morphology and a honeycomb-like texture, which predate the quartz cementation. It is possible that a younger generation of ferruginous cement was coevally formed on the surface or the oxidized zone of the water table, which predated tectonic fractures. In the thickly bedded sandstones altered K-feldspar contains kaolinite and sericite where sericite may be the alteration product from plagioclase mineral inclusion in the K-feldspar. The petrography indicates that the alterations took place

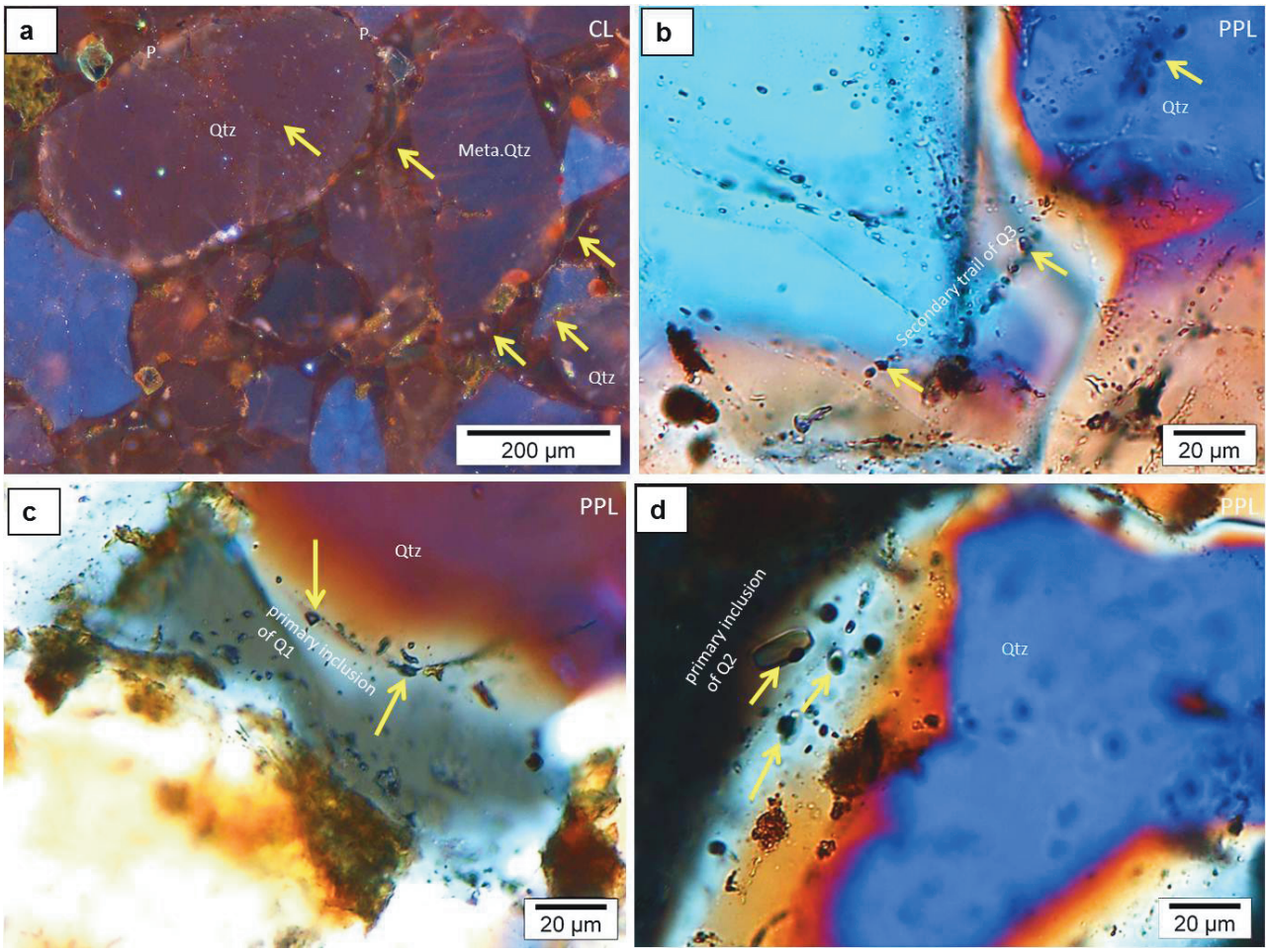

Figure 10. CL image and photomicrographs of fluid inclusions. (a) CL image of fractured detrital quartz grain in the quartz arenite sandstone Q3 (yellow arrow). Pressure solution at a grain contact (P). (b) Fluid inclusion photomicrographs of the same view in (a) showing secondary inclusions of Q3, visible distinctly due to their white-bluish fluorescence (Chalky Nasara section, Sample 16). (c) Fluid inclusions within the quartz cements of primary inclusions of Q1 at the boundary of the detrital quartz grain (yellow arrow) (Ora section, sample 14). (d) Fluid inclusions within quartz rims of primary inclusions of Q2 cement (yellow arrow) (Ora section, sample 14).

prior to the precipitation of authigenic clay and carbonate cement and therefore probably were a result of freshwater near-surface alteration (Figures 4e and 6f).

The late diagenetic stages started by dissolution of carbonate cement and unstable detrital grains such as feldspar and indicate that acidic fluids were flowing freely through most of the sandstones and generated a secondary porosity, which postdated mechanical compaction and clay cement (Figure 6e).

5.2. Sources of quartz cement generations

Different silica sources for quartz cement generations can be active when sediments are subjected to various conditions during diagenesis. This was tested for the sandstones of this study by using hot CL for detrital quartz grains and syntaxial overgrowths, LA-ICP-MS for trace element concentrations, and microthermometric study for fluid inclusions in quartz cement (Tables 4 and 5). Changes in the temperature, pressure, and geochemistry of depositional environments affect the CL properties of quartz grains (Zinkernagel, 1978; Matter and Ramseyer, 1985). Most of the studied detrital quartz grains display a brown or dark brown CL color (Figures 7a and 7b), indicating that they are of low-grade metamorphic origin (Richter et al., 2003). According to Zinkernagel (1978), quartz overgrowths are often nonluminescent. The sharp boundaries of distinct quartz cement phases indicate discontinuous growth, which was interrupted or temporarily extremely slow prior to more rapid growth of the following phase of quartz cement as also observed in five phases of quartz cement in the Ordovician Khabour Formation in northern Iraq (Omer and Friis, 2014). The first quartz cement generation (Q1) was presumably

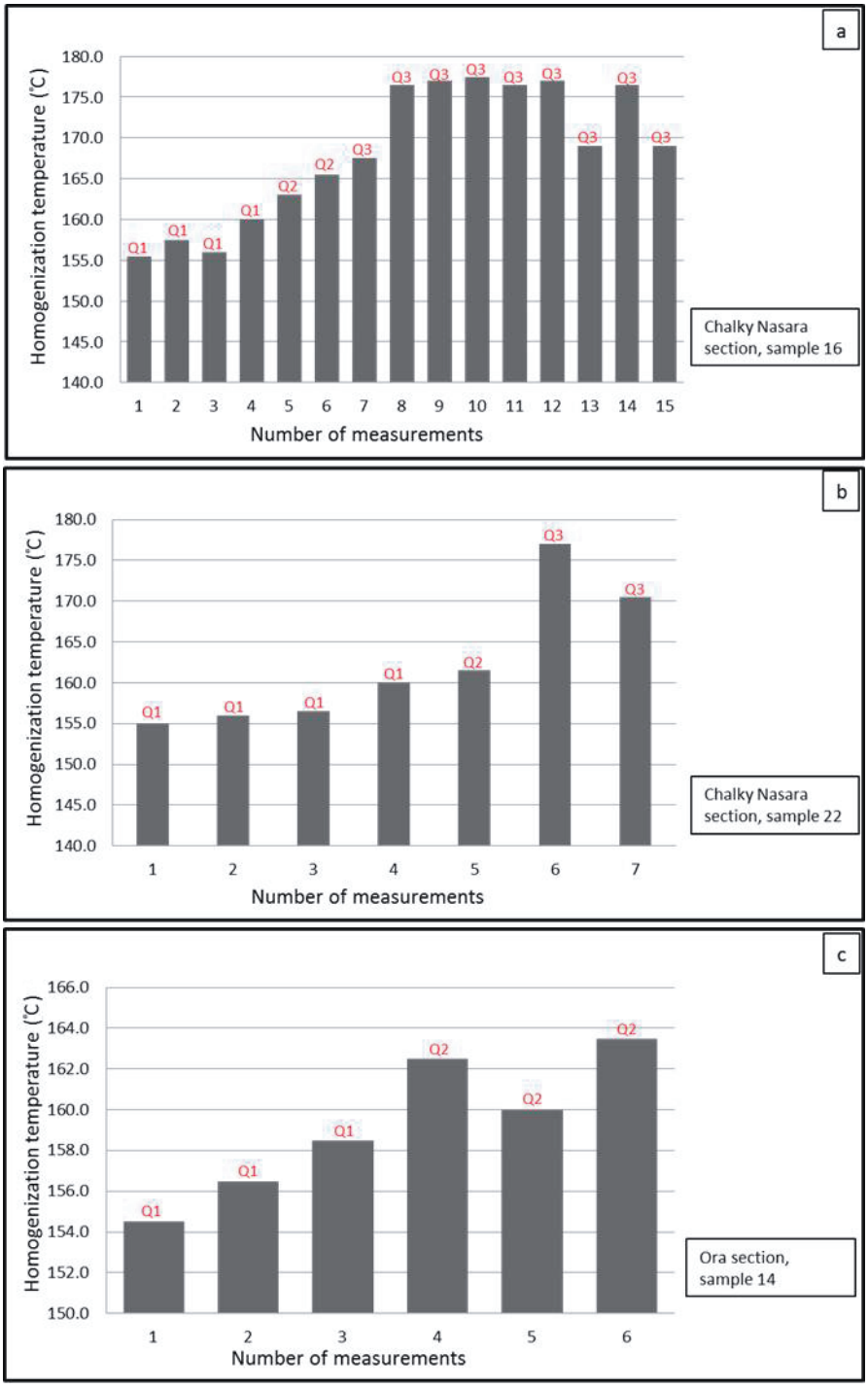

Figure 11. Homogenization temperatures of quartz overgrowths for individual samples. Fluid inclusion homogenization temperatures of each quartz cement generation, Q1, Q2, and Q3, are shown with different patterns from the sandstone of the Ora Formation (Devonian-Carboniferous).

formed together with illite at the expense of feldspar during a relatively early diagenetic stage. Q1 cement is characterized by rims, ranging in thickness from 3 to 30 µm, around detrital quartz grains with low luminescent gray to slightly brown colors (Table 3). This process occasionally leads to reduction in most of the intergranular porosity

around detrital quartz grains and closes permeable surfaces (Figure 7b). The other probable source of quartz cement is the grain-crushing that is developed in two stages; the first one predates the early quartz cement and the second one affected the cracks healed by Q1 cement (Figures 6c and 6d). According to Haddad et al. (2006) and Kraishan et al. (2000), the uniform CL patterns in the quartz cements of sandstone are mostly due to trace element content rather than defects. Based on the work of Kraishan et al. (2000), Weber (2000), and Weber and Ricken (2005), a common source of aluminum in quartz cement is dissolution of feldspar or replacement by clay minerals. The Al concentration in the three quartz cement generations in the Ora Formation is variable (Table 4). The Al concentration in diagenetic quartz cement is controlled by the activity of Al in the aqueous solution, which, assuming equilibrium conditions, is mainly controlled by pH (Marino et al., 1989; Rusk et al., 2008).

The formation of illite as cement during eogenesis and mesogenesis was possibly associated with the formation of Q1 cement generation. Furthermore, the characteristic of other eogenetic quartz cement is the slightly brownish CL color of Q1 cement (Richter et al., 2003). This is supported by the fluid inclusion data for the Q1 cement, which shows moderate homogenization temperatures between 155.0 and 160.0 °C and between 154.5 and 158.5 °C in the Chalky Nasara and Ora sections, respectively (Figures 11a, 11b, and 11c). Salinities for Q1 and Q2 cements are 2.90–3.70 wt.% NaCl equiv. and 3.25–3.87 wt.% NaCl equiv., respectively, in the sandstones from the two sections of the Ora Formation. This is believed to represent moderate meteoric influence on originally saline sea water (Table 5).

The middle-stage quartz cementation (Q2) reaching up to 180 μm in thickness (Table 3) is volumetrically much more important in the thin-bedded sandstone than in the thick-bedded sandstones. The Q2 cementation, which is in places formed as large syntaxial overgrowth, has provided significant contributions to the reduction of porosity and permeability in deeply buried sandstones (Figure 6d) (Weibel et al., 2010). The moderate albitization and alteration of feldspars to kaolinite and sericite, and the dissolution of quartz grains (Figures 4e and 6f) in thick-bedded sandstones, are considered to be sufficient to balance and provide a silica source for this cement generation.

The concentration of Al in quartz, which is strongly controlled by the pH of the solution, reflects its solubility in hydrothermal fluids and thus may be considered as a monitor of pH fluctuations of fluids, especially in the low-temperature type of quartz (Rusk et al., 2008). There is a good correlation coefficient between Al and Li in three quartz cement generations (Figures 8a–8d) with average Li/Al of ~0.02 in Q1 and Q2. This is an indication of the availability of sufficient amounts of both Al and Li. Such a correlation was documented by Demars et al. (1996) for quartz cement that precipitated at a temperature <150 °C; a similar Li/Al ratio was observed in sandstones elsewhere in the world (Demars et al., 1996; Lehmann et al., 2011; Götte et al., 2013). Since illite is the main clay mineral affecting the sandstones of the Ora Formation, the major source of Li is considered to be detrital clays, primarily smectite and illite; this element may be released as a result of interaction of pore water with smectite-illite and illite ripening (Williams and Hervig, 2005). Kaolinite, which is present in some samples, may locally have been replaced by illite at the expense of K-feldspar and excess silica precipitated as quartz cement (Bjørlykke et al., 1989; Bjørlykke and Aagard, 1992). Lithium content of authigenic quartz is thought to be controlled by salinity because of enrichment of Li in high-saline pore waters (Kloppmann et al., 2001; Chan et al., 2002). The average salinity for Q2 quartz cement generation is around 3.4 wt.% NaCl equiv., which is in the range of salinity of sea water.

Following the complete cementation of the sandstones by Q1 and Q2 generations, they were subsequently fractured during telogenesis. The fractures cut detrital grains and all other cements (Figures 7c and 7d), and they were then filled by the Q3 cement generation. However, most of the fractures were filled by chlorite, similar to the phenomenon described by Friis et al. (2010). LA-ICP-MS data of authigenic quartz reveal a significant correlation between Al and Ge, particularly in Q3 cements (Figure 9a). This is an indication that the source of Ge is not related to Al. However, Ge within the detrital quartz grains may be the source of Ge in cement of the Chalky Nasara section. This means that the Ge concentration in the detrital grains is sufficient to provide Ge up to 6.5 ppm in the Q3 quartz cement generation (Table 4). An additional source for Ge is possibly abundant mica flakes (Figure 4f) (Hörmann, 1970) or mica illitization (Evans and Derry, 2002).

Pressure-induced contacts can occur at grain boundaries during advanced burial of siliciclastic rocks (Dutton and Diggs, 1990). The CL images (Figure 10a) show that pressure solution and microstylolites are common in Q3 cement-rich sandstones in the Chalky Nasara section. It is therefore proposed that pressure solutions of detrital quartz and feldspar are the major sources of Ge in Q3 cements (Hartmann et al., 2000a). Analysis of the secondary fluid inclusions of the investigated samples in the Chalky Nasara section showed that the Q3 cement generation has the highest homogenization range, between 167.5 and 177.5 °C with salinity ranging between 5.00 and 6.40 wt.% NaCl equiv., which is much higher than the Th and salinity of the Q1 and Q2 cement generations (Table 5).

Aluminum variations may be caused by changes in the fluid composition (Monecke et al., 2002; Rusk et al., 2008)

and/or changes in the paragenetic assemblage. A specific change of trace element concentration within a few micrometers of hydrothermal quartz has been reported by Rusk et al. (2008) and Jourdan et al. (2009) and was interpreted to have been caused by variations in fluid composition rather than changes in temperature or growth speed. As a second approach to assess our data, cross-plots of the fluid inclusions of the investigated samples between homogenization temperatures (Th) and salinity for the quartz cements revealed three distinct groups representing the three cement generations (Figure 12). The first group (Q1) has lower Th, followed by the second group (Q2), which has slightly higher Th, while the third group (Q3) is characterized by the highest salinity and Th. The salinity of the two first groups (2.9–3.9 wt.% NaCl equiv.) is close to sea water salinity and reflects burial modification of moderate meteoric influence on originally saline sea water. On the other hand, group three has salinity of about twice that of Q1 and Q2, indicating that its precipitation occurred during deep burial conditions of telogenesis.

Rusk et al. (2008) and Müller et al. (2010) suggested that the Al concentration in hydrothermal quartz reflects that Al in the fluid is related to fluid pH, similar to that in Q3 cement. The difference in homogenization regime and brine salinity between Q3 and Q1–Q2 indicates different burial conditions for the Chalky Nasara section and reflects a hydrothermal source for Q3 cement. A hydrothermal source of Q3 cement is supported by the occurrence of Q3 cement in cross-cutting fractures, which often have linings of chlorite and sulfides (Figure 7c).

Trace element compositions and fluid inclusion studies can be used as tools to indicate changes of physicochemical conditions during burial diagenesis of the basin, which further supports the CL results. Fluctuations of the Al content in quartz cement are best explained by changes of CO_2 concentrations in the pore fluids and changes of the paragenetic sequence from quartz-kaolinite to quartz-illite, which is also related to depositional facies.

6. Conclusions

The following conclusions can be drawn from the CL, LA-ICP-MS, and microthermometric studies of the three quartz cement generations (Q1, Q2, and Q3) during the deposition of the Ora Formation in northern Iraq in subtidal, tidal channel, and intertidal flat environments.

1) CL investigation identifies two quartz cement generations (Q1 and Q2) in the Ora section and three quartz cements (Q1, Q2, and Q3) in the Chalky Nasara section.

2) The Q2 quartz cement generation, of dark brown luminescences and up to 180 µm in thickness, is volumetrically a much more important cement generation in the thinly bedded sandstone than in the thickly bedded sandstone facies, which in some cases developed as a large syntaxial overgrowth that has a major influence on reducing porosity and permeability under deep burial conditions. Moderate albitization of feldspar and alteration to kaolinite and sericite is another source for this generation.

3) Fluid inclusion in Q1 and Q2 cements showed similar homogenization temperatures in the two studied sections, whose ranges were between 154.5 and 160.0 °C and 160.0 and 165.5 °C, respectively. Crushed grains and illite were considered the main sources for Q1 cement, while dissolution of feldspar is the source of Q2. Both cements have similar salinity, close to the salinity of sea water.

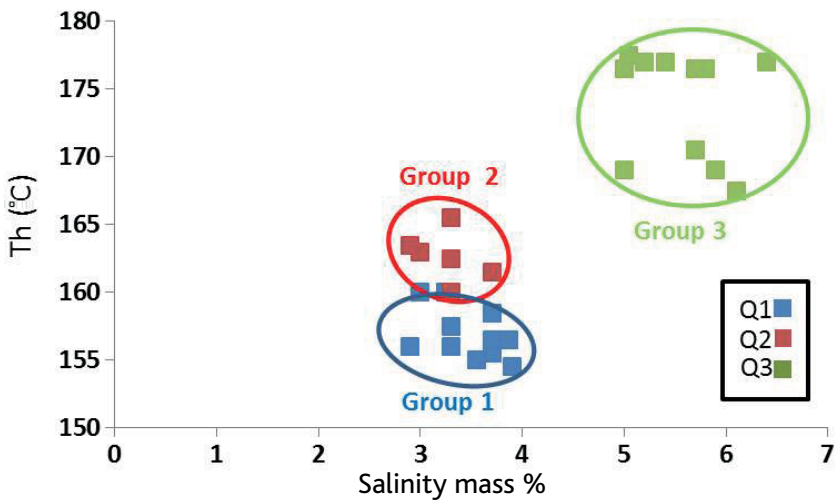

Figure 12. Cross-plots between homogenization temperatures versus salinity of three quartz cements in the quartz arenites of the sandstones of the Ora Formation.

4) The range of homogenization temperatures of the Q3 quartz cement generation formed through telogenesis of deep burial diagenesis was 167.5–177.5 °C, which is higher than those of the Q1 and Q2 quartz generations.

5) Quartz cement generation Q3 formed at higher homogenization temperatures than Q1 and Q2, which were in the range between 167.5 and 177.5 °C, being rather different from other quartz cements and formed through telogenesis of deep burial diagenesis.

6) A significant correlation coefficient was found between Al and Li in the three quartz cement generations with average Li/Al of ~0.02 in Q1 and Q2, independent of total availability of both Al and Li where Li is most likely to have been found in high saline pore waters.

7) A strong positive correlation between Al and Ge, particularly in the Q3 quartz cement generation ($R = 0.889^{++}$), suggests that the pressure solution of detrital grains for supermature quartz arenite and microstylolites at grain margins is the main source for Q3 cement with higher precipitation salinities of 6.10 wt.% NaCl equiv., suggesting hydrothermal precipitation after major thrust fault reaction.

Acknowledgments

The first author would like to thank the Erasmus Mundus Action Program of the European Union for funding this research project as a postdoctorate fellowship, project number SALA1206157, at Warsaw University, Poland. We would like to express our thanks to Professor Boguslaw Bagiński for assistance and for making all SEM research facilities available for this project in the Faculty of Geology, Warsaw University, Poland. Thanks also to Professor Jarosław Stolarski at the Polish Academy of Sciences for making the hot CL available for this study. Furthermore, we are also grateful to helpful Research Associate Dr Hans-Michael Seitz at Goethe University, Frankfurt (Germany), for analyzing trace elements in detrital quartz and cements by LA-ICP-MS.

References

Alavi M (1994). Tectonics of the Zagros Orogenic Belt of Iran: new data and interpretations. Tectonophysics 229: 211-238.

Alavi M (2004). Regional stratigraphy of the Zagros fold-thrust belt in Iran and its proforeland evolution. Am J Sci 304: 1-20.

Alavi M (2007). Structures of the Zagros Fold-Thrust Belt in Iran. Am J Sci 307: 1064-1095.

Al-Hadidy AH (2007). Paleozoic stratigraphic lexicon and hydrocarbon habitat of Iraq. Geo-Arabia 12: 63-130.

Ali SA, Omer M.F, Aqrawi AM (2016). Petrography geochemistry and provenance of the Chalki rocks in Kurdistan region, North Iraq. Arab J Geosci 9: 1-15.

Angevine CL, Turcotte DL (1983). Porosity reduction by pressure solution: a theoretical model for quartz arenites. Geol Soc Am Bull 94: 1129-1134.

Aqrawi AAM, Goff JC, Horbury AD, Sadooni FN (2010). The Petroleum Geology of Iraq. Beaconsfield, UK: Scientific Press Ltd.

Bambauer HU (1961). Spurenelementgehalte und γ-Farbzentren in Quarzen aus Zerrklüften der Sweizer Alpen. Schweiz Miner Petrog 41: 335-369 (in German).

Barzinjy DN (2006). Sedimentology and palynology of Kaista and Ora formations in Zakho area Iraqi Kurdistan Region. MSc, Salahaddin University, Erbil, Iraq.

Basu A (1985). Reading provenance from detrital quartz. In: Zuffa GG, editor. Provenance of Arenites. NATO ASI Series, C 148. Dordrecht, the Netherlands: D. Reidel Publishing Company, pp. 231-247.

Behnam WM (2013). The sedimentology of Ora Formation (Upper Devonian-Lower Carboniferous) in north and west of Iraq. PhD, University of Baghdad, Baghdad, Iraq.

Bellen RC, Dunnington HV, Wetzel R, Morton DM (1959). Lexique Stratigraphique Internal Asia, Fascicule, 10a, Iraq. Paris, France: Central National deal Recherches Scientifique (in French).

Bjørlykke K, Ramm M, Saigal GC (1989). Sandstone diagenesis and porosity modification during basin evolution. Geol Rundsch 78: 243-268.

Bjørlykke K, Aagard P (1992). Clay minerals in North Sea sandstones. Origin, diagenesis and petrophysics of clay minerals in sandstones. SEPM Spec P 47: 65-80.

Buday T (1980). The Regional Geology of Iraq, Stratigraphy and Paleontology. Mosul, Iraq: Dar Al-Kutb Publishing House, University of Mosul.

Chan LH, Starinski A, Katz A (2002). The behavior of lithium and its isotopes in oil field brines: evidence from the Heletz-Kokhov field, Israel. Geochim Cosmochim Ac 66: 615-623.

Davoudzadeh M, Weber-Diefenbach K (1987). Contribution to the paleogeography, stratigraphy and tectonics of the Upper Paleozoic of Iran. Neues Jahrb Geol P-A 175: 121-146.

Demars C, Pagel M, Deloule E, Blanc P (1996). Cathodoluminescence of quartz from sandstones: interpretation of the UV range by determination of trace element distributions and fluid inclusion P-T-X properties in authigenic quartz. Am Mineral 81: 891-901.

Dickinson WW, Milliken KL (1995). The diagenetic role of brittle deformation in compaction and pressure solution, Etjo sandstone, Namibia. Geology 103: 339-347.

Dutton SP, Diggs TN (1990). History of quartz cementation in the Lower Cretaceous Travis Peak Formation, East Texas. J Sediment Petrol 60: 191-202.

Evans MJ, Derry LA (2002). Quartz control of high germanium/silicon ratios in geothermal waters. Geology 30: 1019-1022.

Folk RL, Andrews PB, Lewis DW (1970). Detrital sedimentary rock classification for use in New Zealand. J Geol Geophys 13: 937-968.

Friis H, Sylvestersen RL, Nebel LN, Poulsen MK, Svendsen JB (2010). Hydrothermally influenced cementation of sandstone-An example from deeply buried Cambrian sandstones from Bornholm, Denmark. Sediment Geol 227: 11-19.

Götte T, Pettke T, Ramseyer K, Koch-Müller M, Mullis L (2011). Cathodoluminescence properties and trace element signature of hydrothermal quartz: a fingerprint of growth dynamics. Am Mineral 96: 802-813.

Götte T, Ramseyer K (2012). Trace element characteristics luminescence properties and real structure of quartz. In: Götze J, Möckel R, editors. Quartz: Deposits, Mineralogy and Analytics. Berlin, Germany: Springer, pp. 265-285.

Götte T, Ramseyer K, Pettke T, Müller MK (2013). Implications of trace element composition of syntaxial quartz cements for the geochemical conditions during quartz precipitation in sandstones. Sedimentology 60: 1111-1127.

Haddad SC, Worden RH, Prior DJ, Smalley PC (2006). Quartz cement in the Fontainebleau Sandstone, Paris Basin, France: crystallography and implications for mechanisms of cement growth. J Sediment Res 76: 244-256.

Hartmann BH, Juhász-Bodnár K, Ramseyer K, Matter A (2000a). Polyphased quartz cementation and its sources: a case study from the Upper Paleozoic Haushi Group sandstones, Sultanate of Oman. In: Worden, RH, Morad S, editors. Quartz Cementation in Sandstones. Oxford, UK: International Association of Sedimentologists Special Publication, pp. 253-270.

Hartmann BH, Ramseyer K, Matter A (2000b). Diagenesis and pore-water evolution in Permian sandstones, Gharif Formation, Sultanate of Oman. J Sediment Res 70: 533-544.

Hessami K, Koyi HA, Talbot CJ (2001). The significance of strike-slip faulting in the basement of the Zagros fold and thrust belt. J Petrol Geol 24: 5-28.

Hiatt EE, Kyser TK, Fayek M, Polito P, Holk GJ, Riciputi LR (2007). Early quartz cements and evolution of paleohydraulic properties of basal sandstones in three Paleoproterozoic continental basins: evidence from in situ $\gamma^{18}O$ analysis of quartz cements. Chem Geol 238: 19-37.

Hörmann PK (1970). Germanium. In: Wedepohl KH, Correns CW, Shaw DM, Turekian KK, Zemann J, editors. Handbook of Geochemistry. Berlin, Germany: Springer.

Ingersoll RV, Suczek CA (1979). Petrology and provenance of Neogene sand from Nicobar and Bengal fans, DSDP sites 211 and 218. J Sediment Petrol 49: 1217-1228.

Jassim SZ, Goff JC (2006). Geology of Iraq. Prague, Czech Republic: Dolin.

Jourdan AL, Vennemann TW, Mullis J, Ramseyer K, Spiers CJ (2009). Evidence of growth and sector zoning in hydrothermal quartz from Alpine veins. Euro J Min 21: 219-231.

Kelly JL, Fu B, Kita NT, Valley JW (2007). Optically continuous silcrete quartz cements of the St. Peter Sandstone: high precision oxygen isotope analysis by ion microprobe. Geochim Cosmochim Ac 71: 3812-3832.

Kloppmann W, Négrel P, Casanova J, Klinge H, Schelkes K, Guerrot C (2001). Halite dissolution derived brines in the vicinity of a Permian salt dome (N German Basin), evidence from boron, strontium, oxygen, and hydrogen isotopes. Geochim Cosmochim Ac 65: 4087-4101.

Kraishan GM, Rezaee MR, Worden RH (2000). Significance of trace element composition of quartz cement as a key to reveal the origin of silica in sandstones: an example from the Cretaceous of the Barrow Sub-basin, Western Australia. In: Worden RH, Morad S, editors. Quartz Cementation in Sandstones. Oxford, UK: International Association of Sedimentologists Special Publication, pp. 317-331.

Lehmann K, Pettke T, Ramseyer K (2011). Significance of trace elements in syntaxial quartz cement, Haushi Group sandstones, Sultanate of Oman. Chem Geol 280: 47-57.

Makowitz A, Milliken KL (2003). Quantification of brittle deformation in burial compaction, Frio and Mount Simon Formation sandstones. J Sediment Res 73: 1007-1021.

Marchand AME, Smalley CP, Haszeldine SR, Fallick AE (2002). Note on the importance of hydrocarbon fill for reservoir quality prediction in sandstones. AAPG Bull 86: 1561-1572.

Marino E, Harvey C, Murray HA (1989). Aqueous chemical control of the tetrahedral-aluminum content of quartz, halloysite, and other low-temperature silicates. Clay Clay Miner 37: 135-142.

Matter A, Ramseyer K (1985). Cathodoluminescence microscopy as a tool for provenance studies sandstones. In: Zuffa GG, editor. Provenance of Arenites. NATO Advanced Study Institute Series 148. Dordrecht, the Netherlands: V.C.D. Reidel, pp. 191-211.

McGillivray JG, Husseini MI (1992). The Paleozoic petroleum geology of central Arabia. AAPG Bull 76: 1473-1490.

Merino E, Wang Y, Deloule E (1995). Genesis of agates in flood basalts: twisting of chalcedony fibers and trace element geochemistry. Am J Sci 295: 1156-1176.

Milliken KL, Laubach SE (2000). Brittle deformation in sandstone diagenesis as revealed by scanned cathodoluminescence imaging with application to characterization of fractured reservoirs. In: Pagel M, editor. Cathodoluminescence in Geosciences. Berlin: Germany, Springer, pp. 225-243.

Molenaar N, Cyziene J, Sliaupa S (2007). Quartz cementation mechanisms and porosity variation in Baltic Cambrian sandstones. Sediment Geol 195: 135-159.

Molenaar N, Cyziene J, Sliaupa S, Craven J (2008). Lack of inhibiting effect of oil emplacement on quartz cementation: Evidence from Cambrian reservoir sandstones, Paleozoic Baltic Basin. Geol Soc Am Bull 120: 1280-1295.

Monecke T, Kempe J, Götze J (2002). Genetic significance of the trace element content in metamorphic and hydrothermal quartz: a reconnaissance study. Earth Planet Sci Lett 202: 709-724.

Morad S, Ketzer JM, De Ros LF (2000). Spatial and temporal distribution of diagenetic alterations in siliciclastic rocks: implications for mass transfer in sedimentary basins. Sedimentology 47: 95-120.

Müller A, Herrington R, Armstrong R, Seltmann R, Kirwin DJ, Stenina NG, Kronz A (2010). Trace elements and cathodoluminescence of quartz in stockwork veins of Mongolian porphyry-style deposits. Miner Deposita 45: 707-727.

Müller A, Wiedenbeck M, Van den Kerkhoff AM, Kronz A, Simon K (2003). Trace elements in quartz - a combined electron microprobe, secondary ion mass spectrometry, laser ablation ICP-MS, and cathodoluminescence study. Eur J Mineral 15: 747-763.

Neuser RD, Bruhn F, Gtöze J, Habermann D, Richter DK (1996). Kathodolumineszenz: Methodik und Anwendung: Zentralblatt fur Geologie und Palaontologie, Teil I, H. 1/2. Stuttgart, Germany: Schweizerbart and Borntraeger (in German).

Omer MF (2012). The sedimentology and geochemistry of the Khabour Formation Northern Iraq. PhD, University of Baghdad, Baghdad, Iraq.

Omer MF (2015). Cathodoluminescence petrography for provenance studies of the sandstones of Ora Formation (Devonian-Carboniferous), Iraqi Kurdistan Region, northern Iraq. J Afr Earth Sci 109: 195-210.

Omer MF, Friis H (2014). Cathodoluminescence investigations on quartz cement in the sandstones of Khabour Formation from Iraqi Kurdistan Region, Northern Iraq. J Afr Earth Sci 91: 44-54.

Postma D (1982). Pyrite and siderite formation in brackish and freshwater swamp sediments. Am J Sci 282: 1151-1183.

Rezaee M, Tingate PR (1997). Origin of quartz cement in Tirrawarra Sandstone, Southern Cooper Basin, South Australia. J Sediment Res 67: 168-177.

Richter DK, Götte T, Götze J, Neuser RD (2003). Progress and application of cathodoluminescence in sedimentary petrology. Mineral Petrol 79: 127-166.

Roedder E (1984). Fluid Inclusions. Reviews in Mineralogy, Vol. 12. Chantilly, VA, USA; Mineralogical Society of America.

Rusk BG, Lowers HA, Reed MH (2008). Trace elements in hydrothermal quartz: relationships to cathodoluminescent textures and insights into vein formation. Geology 36: 547-550.

Scholle PA (1979). A Color Illustrated Guide to Constituents, Textures, Cements, and Porosities of Sandstones and Associated Rocks. Tulsa, OK, USA: AAPG Memoirs.

Sharland PR, Archer R, Casey DM, Hall SH, Heward AP, Horbury AD, Simmons MD (2001). Arabian Plate Sequence Stratigraphy. Geo Arabia, Special Publications 2. Manama, Bahrain: Gulf Petrolink.

Sibley DF, Blatt H (1976). Intergranular pressure solution and cementation of the Tuscarora orthoquartzite. J Sediment Petrol 46: 881-896.

Sissakian V (2000). Geological Map of Iraq, Scale 1:1,000,000. 3rd ed. Baghdad, Iraq: GEOSURV.

Stocklin J (1968). Structural history and tectonics of Iran: a review. AAPG Bull 52: 1229-1258.

Stocklin J (1974). Possible ancient continental margins in Iran. In: Burk CA, Drake CL, editors. The Geology of Continental Margins. Berlin, Germany: Springer-Verlag, pp. 873-887.

Tada R, Sieve R (1989). Pressure solution during diagenesis. Ann Rev Earth Pl Sc 17: 89-118.

Takin M (1972). Iranian geology and continental drift in the Middle East. Nature 235: 147-150.

Talebian M, Jackson J (2004). A reappraisal of earthquake focal mechanisms and active

shortening in the Zagros Mountains of Iran. Geophys J Int 156: 506-526.

Tamar-Agha MY (2009). The influence of cementation on the reservoir quality of the Risha Sandstone Member (Upper Ordovician), Risha Gasfield, NE Jordan. J Petrol Geol 32: 193-208.

Taylor TR, Giles MR, Hathon LA, Diggs TN, Braunsdorf NR, Birbiglia GV, Kittridge MG, Macaulay CI, Espejo IS (2010). Sandstone diagenesis and reservoir quality prediction: Models, myths, and reality. AAPG Bull 98: 1093-1132.

Tortosa A, Palomares M, Arribas J (1991). Quartz grain types in Holocene deposits from the Spanish Central System: some problems in provenance analysis. In: Morton AC, Todd SP, Haughton PDW, editors. Developments in Sedimentary Provenance Studies. London, UK: Geological Society of London Special Publications, pp. 47-54.

Van den Kerhof AM, Scherer T, Riganti A (1996). Cathodoluminescence and EPR analysis of Archean quarzites from the Nondweni Greenstone Belt, South Africa. In: Abstracts of the SLMS International Conference on Cathodoluminescence, p. 75.

Walderhaug O (1994). Precipitation rates for quartz cement in sandstones determined by fluid-inclusions microthermometry and temperature history modeling. J Sediment Res 64: 324-333.

Weber J (2000). Kieselsäurediagenese und gekoppelte Sedimentarchitektur - eine Beckenanalyse des Reinhardswald-Troges (Norddeutsches Becken, Solling-Folge, Mittlerer Buntsandstein). PhD, University of Cologne, Cologne, Germany (in German).

Weber J, Ricken W (2005). Quartz cementation and related sedimentary architecture of the Triassic Solling Formation, Reinhardswald Basin, Germany. Sediment Geol 175: 459-477.

Weibel R, Friis H, Kazerouni AM, Svendsen JB, Stokkendal J, Poulsen MLK (2010). Development of early diagenetic silica and quartz morphologies-Examples from the Siri Canyon, Danish North Sea. Sediment Geol 228: 151-170.

Williams LB, Hervig RL (2005). Lithium and boron isotopes in illite-smectite: the importance of crystal size. Geochim Cosmochim Ac 69: 5705–57.

Worden RH, Morad S (2000). Quartz cementation in oil field sandstones: a review of the key controversies. In: Worden RH, Morad S, editors. Quartz Cementation in Sandstones. Oxford, UK: International Association of Sedimentologists Special Publication, pp. 1-20.

Zhang J, Qin L, Zhang Z (2008). Depositional facies, diagenesis and their impact on the reservoir quality of Silurian sandstones from Tazhong area in central Tarim basin, western China. J Asian Earth Sci 33: 42-60.

Zinkernagel U (1978). Cathodoluminescence of Quartz and Its Application to Sandstone Petrology. Contributions to Sedimentary Geology, Volume 8. Stuttgart, Germany: Schweizerbart and Borntraeger.